Macromolecules

pubs.acs.org/Macromolecules Article

Thermodynamics and Structure of Poly[*n*]catenane Melts

Phillip M. Rauscher, Kenneth S. Schweizer, Stuart J. Rowan, and Juan J. de Pablo*

Cite This: *Macromolecules* 2020, 53, 3390−3408 Read Online

ACCESS | Metrics & More | Article Recommendations

ABSTRACT: Motivated by recent achievements in the synthesis of interlocking polymers, the structural features of poly[*n*]catenanes, polymers composed entirely of interlocking rings (or macrocycles), are studied by extensive molecular dynamics simulations in the melt state. The degree of polymerization (number of links) is varied from $n = 1-25$ and the number of beads per macrocycle is varied from $m = 15-50$; the results are compared to linear chains of degrees of polymerization $N = 15-175$. The mechanical bonds in the system cause significant topological contributions to the pressure and potential energy density not seen in other polymer systems. The polymers themselves possess many unusual structural features at short and intermediate length scales, which can be attributed to density inhomogeneities along the polymer contour. Furthermore, the conformations of the individual macrocycles within poly[*n*]catenanes are quite different from those of ordinary ring polymers and depend on the topology of the macrocycle, that is, whether it is threaded by one ring (chain end) or two (chain center). At larger length scales, the poly[*n*]catenanes are conformationally similar to ideal linear chains, but unlike traditional (covalent) polymers, they are highly globular at low degrees of polymerization and are extremely flexible relative to their size, which inhibits interchain entanglement. Implications for poly[*n*]catenane material properties and synthesis are discussed.

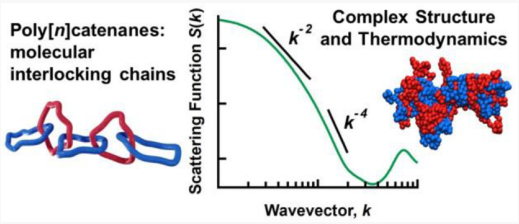

1. INTRODUCTION

Polymer liquids are often dominated by topological interactions, which arise because chains cannot pass through one another.[1] These topological constraints do not greatly affect small chains since the interactions are transient and the relevant time and length scales are quite short. However, for systems of long chains, the polymers are severely restricted in their motion by the neighboring chains. These restrictions greatly increase polymer relaxation times and dramatically alter diffusion and rheological behavior.[1,2] Over the past few decades, many theories have attempted to explain and predict the effects of topological interactions in linear polymer systems, for instance, the phenomenological tube/reptation,[3−8] and slip-link[9−14] models, or more fundamental force-level theories.[15−18] Despite these impressive effects on dynamical behavior, linear polymers do not show any meaningful changes in melt structure or chain conformations associated with the onset of entanglement, either at the intra- or intermolecular level, as shown by experiment[19−21] and simulation.[2,22,23] Thus, the topological interactions do not disallow any chain or system configurations but instead prevent certain dynamical paths between them. To connect structure and dynamics, authors have attempted to formulate microscopic definitions of an "entanglement" so that molecular simulations could be used to unambiguously identify such topological interactions and analyze their statistics and dynamics.[24−33] However, researchers have yet to reach consensus about how entanglements should be defined and what kinds of relative chain conformations constitute them. On account of these challenges, linear polymers and their topological interactions remain an active subject of research.

Nonconcatenated (unlinked) ring polymers present an entirely distinct challenge since topological interactions manifest themselves very differently in these systems. For example, linear polymers do not show changes in structural features, including scaling of radius of gyration, R_g, due to entanglement, as mentioned above. However, at intermediate molecular weight, ring polymers in the melt appeared to scale in size according to $R_g \sim N^{2/5}$ owing to the topological interactions in early work,[34−40] although more recent studies have demonstrated that this is not a true scaling regime but rather a crossover between ideal scaling at small N and collapsed, globule-like scaling at large N, $R_g \sim N^{1/3}$.[38,41−43] The topological interactions also affect the dynamics in a unique way in ring polymer melts. Although the diffusion constants scale similarly to those of entangled linear polymers: $D \sim N^{-a}$ with $a \approx 1.9-2.3$ (a major puzzle),[39,41,42,44] the stress relaxation modulus shows no rubbery plateau and polymer relaxation times scale much more slowly than those of

Received: December 23, 2019
Revised: March 10, 2020
Published: March 27, 2020

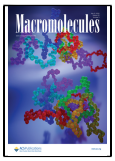

https://dx.doi.org/10.1021/acs.macromol.9b02706
Macromolecules 2020, 53, 3390−3408

entangled linear polymers, suggesting a decoupling of internal and center-of-mass dynamics.[43−48] These differences between linear and ring polymer systems can be attributed to the fact that the topological interactions are quite different in the two systems. While linear polymers can interpenetrate each other freely, ring polymers cannot, as they must remain non-concatenated, prohibiting certain configurations. As a result, the topological interactions affect both structure and dynamics in ring polymer systems, as opposed to linear polymer systems in which only dynamics are impacted. This kind of non-concatenation constraint has been studied theoretically for quite a long time using topological invariants such as the Gauss linking number.[49,50] For instance, these constraints are known to lead to a positive second virial coefficient, even when excluded volume interactions disappear.[51−53] On the basis of this observation, ring polymer melts should exhibit topological contributions to thermodynamic quantities such as the pressure, but these effects have not yet been observed.[38]

Taking polymer architecture a step further, mechanically interlocking polymers (MIPs) have seen enormous growth in preparation and study over the last few decades. Unlike the linear and ring polymers discussed above, these systems possess permanent topological interactions in the form of mechanical bonds. Such mechanically bound polymers contain components that are not covalently bound but cannot be separated without breaking a covalent bond.[54,55] The precise topological character of the mechanical bond can take many forms, for instance, Hopf[56] or Solomon[57−59] links or Borromean rings.[60,61] The most commonly synthesized MIPs are polyrotaxanes and polycatenanes,[62,63] and such polymers have been applied as high-performance materials and molecular machines.[64,65] Because of the mechanical bonds within these polymers, such systems may also serve as model systems for studying the effects of specific kinds of topological interactions. Among the most intriguing of these systems are poly[n]catenanes, which were recently synthesized for the first time.[66] These polymers are composed solely of interlocking ring molecules (or macrocycles) arranged in a linear fashion and are therefore dominated by mechanical bonds (Figure 1). For many decades, researchers have speculated that poly[n]-catenanes would exhibit a variety of unusual behaviors.[54,63,65] In particular, it has been suggested that polycatenanes could exhibit "high loss modulus, rapid stress relaxation, and low activation energy for viscous flow".[54] While such potential properties have motivated many chemists to target poly-catenanes synthetically,[65,66] to date no rheological studies have been carried out to confirm such claims, and only a few theoretical or computational studies have been conducted.[67−69] As a result, the static and dynamic properties of poly[n]catenanes are not well understood at this time. As poly[n]catenane synthesis remains an active area of research, a better understanding of the melt state properties of these polymers will help chemists design and target the most promising candidates for new materials. Reported herein are computational studies focused on the thermodynamics and structural properties of model poly[n]catenane systems in the liquid state.

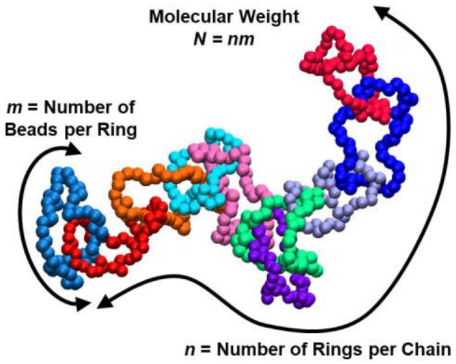

Figure 1. Visualization of a poly[n]catenane. For clarity, each ring is colored differently. The variable m indicates the number of beads per ring, while n denotes the number of rings per chain, as shown. For this molecule, n = 10 and m = 50. Note that this configuration was obtained during system preparation at very low density, similar to good solvent conditions, so that the interlocking structure can be more clearly observed; poly[n]catenanes in the melt are much more collapsed/globular (Figure 9b).

There are a limited number of computational/theoretical studies on poly[n]catenanes, and all of them have focused on simulating isolated molecules under conditions akin to dilute solution in good solvent. The polymers were first studied using an athermal lattice-based Monte Carlo method, examining a variety of ring sizes and chain lengths.[67] The polymer radius of gyration and end-to-end distance obeyed the same scaling relations, $R_g \sim R_e \sim N^{\nu}$, as ordinary linear polymers in good solvent ($\nu \approx 3/5$) and the data collapsed to a master curve when normalized by the size of the individual rings, suggesting that poly[n]catenanes could be renormalized to linear polymers at large length scales, which was also suggested by later theoretical work.[69] The polymers also exhibited highly complex single-chain structure factors and unusual dynamics. However, for the smaller ring sizes in the study, the mechanical bonds were comparable in length to the lattice spacing, which may artificially limit the available conformations, introducing artifacts, particularly with regards to the dynamics. Indeed, an early study of [2]catenanes using another lattice model pointed out such difficulties.[70] To circumvent these issues, we recently conducted molecular dynamics (MD) simulations of isolated poly[n]catenanes using the Kremer-Grest (KG) model.[68] Our results agree with the earlier work at large length scales and furthermore indicate that larger ring sizes lead to more flexible catenanes, relative to the length of the mechanical bond. However, at short length scales, the conformations of the rings within catenanes are strongly affected by the mechanical bonds, which are quantified in terms of the Rouse mode amplitudes.[71,72] More specifically, the rings are expanded at large length scales but compressed at smaller ones compared to rings without threadings. Since then, additional simulations were conducted by other researchers[73] also using the KG model, extending the chain lengths up to n = 100 rings. These extremely long poly[n]catenanes showed highly unusual structural properties including unexpected scaling behavior and large, long-lived orientational correlations along the chain. However, the simulation times appear to be short relative to the relaxation times of the polymers (and in some cases only half as long) so the results may be complicated by inadequate sampling.

In the dense melt state, poly[n]catenanes are completely unstudied. However, the behavior of linear and ring polymers in the melt combined with the properties of these polymers in good solvent conditions suggests a number of questions: (1) does the mechanical bond contribute to the stress/pressure and other thermodynamic quantities?, (2) is it possible to

https://dx.doi.org/10.1021/acs.macromol.9b02706
Macromolecules 2020, 53, 3390−3408

further quantify how the topological bond impacts macrocycle conformations?, (3) how does ring size affect the conformation and scaling of catenanes?, (4) how do intermolecular interactions and the unusual intramolecular conformational structure affect poly[n]catenane melt packing correlations?, (5) what is the interplay between intra- and intermolecular topological interactions?, and (6) at what point is interchain entanglement important in poly[n]catenane systems? This study aims to answer the above questions (and others) by performing extensive molecular dynamics simulations of poly[n]catenane melts. Both the degree of polymerization (i.e., the number of links), n, and the ring size, m, are varied, and the results are compared to linear polymer and unlinked ring (n = 1) melts. As many different systems have been simulated, it is a challenge to present the entirety of the data in a clear and concise manner. Therefore, this paper will be representative and illustrative rather than exhaustive.

2. SIMULATION METHODS

As in our previous work,[68] the Kremer-Grest (KG) model[2] is employed. All macrocycles in all catenanes are composed of identical beads of mass μ, which interact with one another via a shifted Lennard-Jones (LJ) potential:

$$U_{\text{pair}}(r_{ij}) = \begin{cases} 4\epsilon\left[(\sigma/r_{ij})^{12} - (\sigma/r_{ij})^{6}\right] + \epsilon, & r_{ij} \le 2^{1/6}\sigma \\ 0, & r_{ij} > 2^{1/6}\sigma \end{cases} \quad (1)$$

Covalent bonds within ring molecules are enforced by a finitely extensible nonlinear elastic (FENE) potential:

$$U_{\text{bond}}(r_{ij}) = \begin{cases} -0.5kR_0^{\,2}\ln[1 - (r_{ij}/R_0)^2], & r_{ij} \le R_0 \\ \infty, & r_{ij} > R_0 \end{cases} \quad (2)$$

where parameter values of $k = 30\varepsilon/\sigma^2$ and $R_0 = 1.5\sigma$ are chosen. No bond angle bending potential is applied, so the ring molecules are fully flexible. These interaction potentials along with the indicated parameters have been shown to prevent chain crossings,[2] which is crucial for the simulation of interlocking polymers. The poly[n]-catenanes are held together only by the topological linking, which is specified entirely by the initial configurations of the beads and maintained only by the interaction potentials in eqs 1 and 2. The velocity-Verlet algorithm was used to integrate the equations of motion with a time step of $\delta t = 0.01\tau$ where $\tau = (\mu\sigma^2/\varepsilon)^{1/2}$ is the LJ unit of time. The simulations are conducted at a number density of $\rho = 0.85\sigma^{-3}$ and a temperature of $T = 1.0\varepsilon/k_B$, maintained via a Langevin thermostat with a drag coefficient of $\Gamma = 0.5\mu/\tau$. All results are reported in reduced LJ units. Simulations were conducted with the GPU-accelerated MD engine DASH.[74]

The systems studied here contain a total number of poly[n]-catenane molecules of $\mathcal{N}$ = 100−500, with the number of rings in each polymer, n, varied between n = 1, 2, 3, 5, 7, 10, 15, 20, and 25. For each chain length, catenanes with a number of beads-per-ring, m, varied between m = 15, 20, 30, and 50, are considered. Thus, the total molecular weight, $N = nm$, ranges from 15 to 1250. Note that these ring sizes are considerably smaller than the entanglement length of the KG model ($N_e \approx 85$),[26] so no significant intermolecular topological compression is expected between the rings.[38,44] A poly[n]catenane with n = 10 and m = 50 is depicted in Figure 1. Linear polymer systems with $\mathcal{N}$ = 500 and degree of polymerization N varying between N = 15, 20, 30, 45, 60, 80, 100, 150, and 175 have also been simulated for comparison. For statistical analysis, five independent simulations of each system were conducted. Production simulations were run for 10^6−10^7 τ, depending on polymer size. More details concerning the poly[n]catenane and linear polymer systems and the simulation preparation procedures may be found in Appendix A, along with quantitative analysis confirming system equilibration.

3. THERMODYNAMIC PROPERTIES

Topological interactions can affect the pressure in certain polymer systems. For example, in unlinked ring polymers, the topological interactions cause the chains to repel each other weakly.[51−53,75] In the melt, these interactions should increase the pressure relative to linear polymers, but such an increase has not been observed in simulations of high-MW ring polymer melts,[38] likely because such effects are more subtle for these systems. Nevertheless, topological effects may also contribute to the pressure in poly[n]catenane melts, but in the opposite manner. The rings must be linked and are therefore prevented from separating from one another, so they effectively attract each other. Thus, the pressure should decrease as the number (or concentration) of mechanical bonds increases, even if the concentration of covalent bonds

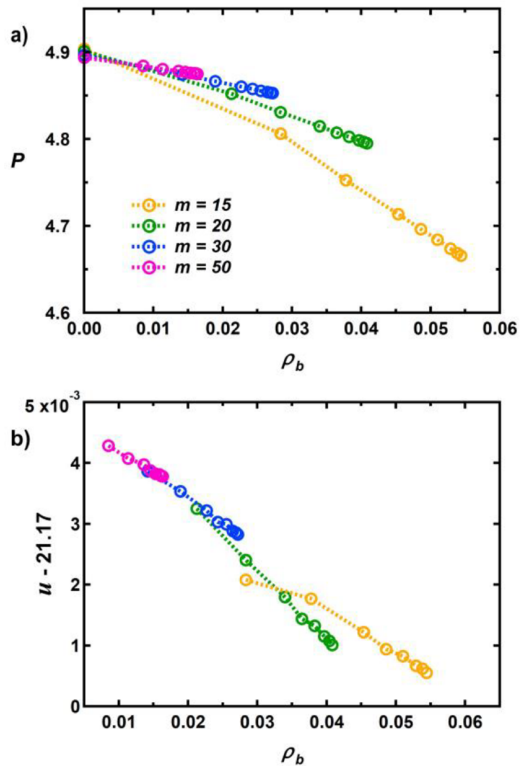

Figure 2. (a) Pressure and (b) potential energy per particle as a function of the density of mechanical bonds (eq 3) for poly[n]-catenanes with various m. The statistical errors are approximately equal to the size of the data points. Note that in panel b, a common factor has been subtracted from the values to more clearly visualize the trend; also the spacing between tick marks on the vertical axis is only $10^{-3}\varepsilon$, so the differences in energy are quite small.

does not change. Figure 2a shows the pressure as a function of the number density of mechanical bonds, defined as

$$\rho_b \equiv \frac{\mathcal{N}(n-1)}{V} = \rho\frac{n-1}{nm} \quad (3)$$

recalling that ρ is the number density of beads in the melt. The pressure is calculated according to the virial theorem:

https://dx.doi.org/10.1021/acs.macromol.9b02706
Macromolecules 2020, 53, 3390−3408

Table 1. Structural Properties of Macrocycles[a]

	M	$R_{g,r}^2$	$\nu_{g,r}(m)$	R_d^2	$\nu_d(m)$	α	$\langle\lambda_1\rangle:\langle\lambda_2\rangle:\langle\lambda_3\rangle$
free rings	15	2.06		6.93		−0.18	1.0:2.7:6.5
	20	2.77	0.51	9.15	0.48	−0.15	1.0:2.5:6.3
	30	4.14	0.50	13.26	0.46	−0.11	1.0:2.4:6.2
	50	6.75	0.48	21.0	0.45	−0.08	1.0:2.3:6.1
chain ends	15	2.54		9.06		−0.28	1.0:4.4:8.5
	20	3.31	0.46	11.6	0.42	−0.24	1.0:3.5:7.5
	30	4.77	0.45	15.9	0.40	−0.18	1.0:2.8:6.8
	50	7.49	0.44	23.8	0.40	−0.12	1.0:2.5:6.3
chain centers	15	3.01		11.14		−0.32	1.0:6.4:11.5
	20	3.89	0.45	14.1	0.42	−0.28	1.0:4.7:9.3
	30	5.53	0.43	19.1	0.38	−0.22	1.0:3.5:7.7
	50	8.50	0.42	27.9	0.37	−0.15	1.0:2.8:6.8

[a]Data taken from poly[n]catenanes (n = 7) and free rings (n = 1). Mean square radius of gyration ($R_{g,r}^2$), apparent scaling exponent (calculated from the radius of gyration via finite difference, $\nu_{g,r}$), mean square diameter vector (R_d^2), apparent scaling exponent (calculated from the diameter vector via finite difference, ν_d), non-Gaussian parameter of the diameter vector distribution (α, see eq 5), and ratio of average gyration tensor eigenvalues ($\langle\lambda_1\rangle:\langle\lambda_2\rangle:\langle\lambda_3\rangle$). Statistical uncertainties occur in the decimal places after those reported.

$$P = \rho k_B T + \frac{1}{3V}\left\langle \sum_{j>i} \boldsymbol{F}_{ij}\cdot\boldsymbol{r}_{ij} \right\rangle \tag{4}$$

where V is the system volume, $\boldsymbol{F}_{ij}$ is the force exerted on particle i by particle j, $\boldsymbol{r}_{ij} = \boldsymbol{r}_j - \boldsymbol{r}_i$ is the vector between the particle positions, and the sum runs over all pairs of particles in the system. As expected, the pressure decreases as ρ_b increases, reaching values up to 5% lower than those of ring polymers. In analogy with the virial pressure given above (eq 4), such decreases typically indicate that more attractive forces are present within the system. The only attractive forces that are specified by the molecular model are the covalent bonds (eq 2). However, in all cases, each Lennard-Jones bead is bonded to exactly two others, so the concentration of such bonds is constant, irrespective of ρ_b. Also, the beads only interact repulsively via a truncated LJ potential (eq 1) and therefore cannot lower the pressure unless the particle density is also reduced (and it is not). In general, the Hamiltonian is the same for all systems along with the density and temperature, so any changes in the pressure must be related to changes in the integration limits (rather than the statistical weights) of the partition function, that is, they must be caused by the topological constraints/bonds. In other words, the mechanical bonds introduce effective (topological) attractions between linked rings, even though the actual forces are purely repulsive; these attractions in turn modify the pressure. Evidently, the topological attraction between linked rings is much stronger than the topological repulsions between nonconcatenated rings since pressure increases have not been observed in simulations of nonconcatenated ring polymer melts.[38] In any case, such repulsions should not be important for the small rings considered here compared to ordinary excluded volume (i.e., that arising from the finite volume of the beads) since the rings are much smaller than the entanglement length of the KG model, m < Ne. For n > 2, the pressure decreases linearly with ρ_b, with the largest effects observed for the smallest rings. The dependence on ring size may be related to the fact that the bond length distributions for small rings are more sharply peaked, which would typically lead to stronger effective forces between the macrocycles. However, these distributions lead to potentials of mean force, which are highly anharmonic (not shown), precluding any simple interpretation. Since a constant slope is only observed when n > 2, the doubly threaded rings apparently contribute more strongly to the pressure than the singly threaded ones.

The potential energy per particle, $u \equiv U/\mathcal{N}N$, also decreases linearly with ρ_b, as shown in Figure 2b, but the differences are much smaller than those seen in the pressure, being less than 1% of the value (but still larger than statistical uncertainty). The potential energy is obtained by time-averaging the instantaneous potential energy of the system calculated at regular intervals. In contrast to the pressure, u does not depend strongly on m, which can be rationalized in terms of an equipartition theorem. In a crude sense, the mechanical bond forces the centers-of-mass of two rings to remain close to each other, removing a degree of freedom (without actually altering the Hamiltonian). On average, this degree of freedom will be associated with some potential energy, which depends on the temperature, and if the internal degrees of freedom of the rings are not affected, then this energy will not depend on m. Denoting this energy by $A(T)$ and assuming that these degrees of freedom are independent, the change in potential energy associated with adding mechanical bonds to the system, ΔU, will be proportional to the number of mechanical bonds: $\Delta U \approx A(T)\mathcal{N}(n-1)$. Dividing this quantity by $\mathcal{N}N$, the total number of particles, leads to a linear relation between the potential energy and the concentration of mechanical bonds,

$$\Delta u \approx A(T)(n-1)/nm = A(T)\rho_b/\rho$$

The total system potential energy has both intra- and intermolecular contributions, which can be related to the appropriate site−site pair correlation function. Thus, the small changes in per-particle potential energy (Figure 2b) must be accompanied by small changes in the fluid structure. Indeed, the site−site correlation function can be used to numerically obtain energy differences in agreement with those of Figure 2 (not shown). However, the actual correlation functions themselves are indistinguishable to the eye, which is unsurprising given the smallness of the energy differences. Moreover, these correlation functions agree quantitatively with

https://dx.doi.org/10.1021/acs.macromol.9b02706
Macromolecules 2020, 53, 3390−3408

those of linear polymers of high-MW where chain ends effects become negligible. For very small ring sizes (not discussed here), the fluid structure can indeed be significantly affected by chain length, n, which introduces a number of unusual static and dynamic properties. Such systems will be discussed in a separate work.

The results presented in this section represent some of the largest topological effects yet observed in bulk thermodynamic properties of polymer systems. In particular, the system pressure shows a strong dependence on the ring size, m, suggesting that topological effects in poly[n]catenanes will be most prevalent for smaller ring sizes. In other words, the concatenation between rings may restrict the available ring conformations more severely for smaller rings. There is also a strong dependence on the number of rings in each catenane, n, which modifies the number of mechanical bonds (i.e., concatenation constraints). To more fully understand poly[n]catenane systems, it is therefore necessary to study the conformational properties of the polymers both in terms of individual rings and at the level of the overall chain. These properties are the subject of the next two sections.

4. RING CONFORMATION

When studying the conformations of individual macrocycles within poly[n]catenanes, chain centers and chain ends must be handled separately since the former are threaded by two rings while the latter are threaded by only one; these rings should also be compared with free ring polymers (n = 1), which are not threaded by any other rings. It was found that the ring conformations do not depend on n for catenanes of $n \geq 5$, and all quantities are therefore calculated from chains of length n = 7 for simplicity. Table 1 displays some structural properties of the rings. As expected, mechanical bonds increase the single macrocycle size relative to that of free rings for all values of m, as measured by both the mean squared radius of gyration, $R_{g,r}^2$ (the second subscript "r" indicating that this quantity applies to individual rings), and the mean squared diameter vector, R_d^2. The ratio $R_{g,r}^2/R_d^2$ should equal 1/3 for ideal Gaussian ring polymers and 1/4 for perfectly rigid circles. The observed ratios are indeed close to the Gaussian value for free ring polymers, with larger rings having more ideal conformations and smaller ones deviating slightly. Chain ends and chain centers deviate more strongly from ideal behavior with ratios as small as 0.27 observed for the smallest rings, suggesting that the mechanical bond leads to effectively stiffer polymer segments and more circular conformations.

Ideal (phantom) ring polymers without topological restrictions have a Gaussian-distributed diameter vector,[71,76] and real ring polymers in the melt generally obey such a distribution, even when topological interactions cause nonideal scaling of the ring size.[38] However, this distribution may be affected by the mechanical bonds in poly[n]catenanes for the small ring sizes studied here. This effect can be quantified by a non-Gaussian parameter:

$$\alpha \equiv \frac{3\langle R_d^4\rangle}{5\langle R_d^2\rangle^2} - 1 \tag{5}$$

, which takes on a value of zero if the diameter vector is Gaussian-distributed and −0.4 if it is delta-function distributed. All systems exhibit negative parameters, but the values tend toward zero with increasing ring size m, achieving nearly ideal statistics for the largest free rings (m = 50, Table 1). At small m, the negative values of α suggest that the conformational freedom of the rings is limited by the topological restriction that the loop be closed. In general, the mechanical bonds further reduce the non-Gaussian parameters, again indicating stiffer polymers, which is consistent with the larger ring sizes discussed above.

The mechanical bonds also affect the shape of the rings, which can be determined by the ratio of the eigenvalues of the gyration tensor, also shown in Table 1. As expected, unthreaded rings show very similar shape for all m since they are nearly ideal ring polymers. Threaded rings, however, are highly distorted by the mechanical bonds, particularly at small m, where they adopt nearly two-dimensional shapes as indicated by the large increases in the eigenvalue ratios. These shape changes are also observed in the ring density profiles as a function of the distance from the center-of-mass, shown in Figure 3. While the unthreaded rings show (nearly)

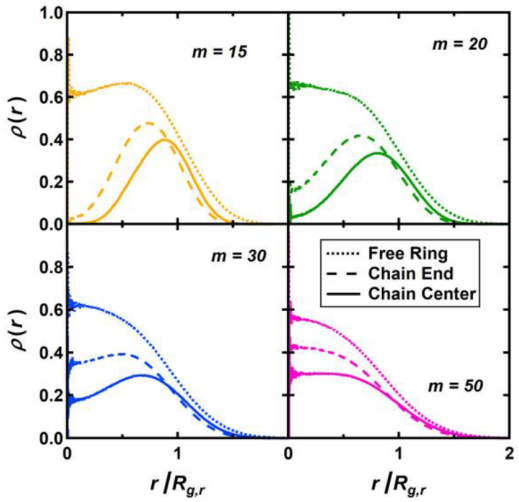

Figure 3. Ring density profile as a function of distance from macrocycle center-of-mass for poly[n]catenanes and ring polymers. Note that the legend in the lower right pane applies to all graphs.

monotonically decreasing density profiles for all ring sizes, the threaded rings exhibit large depletions near the center of mass and form toroidal shapes. As expected, the magnitude of this effect decreases as the ring size m increases.

As discussed in the Introduction, the size of ring polymers scales more slowly with molecular weight in the melt compared to linear polymers or ideal Gaussian rings. Since this unusual scaling is driven by topological interactions, the mechanical bonds are expected to alter the scaling of ring size within the poly[n]catenanes. Of course, the rings considered here are rather small, with ring size, m, being considerably less than the typical (linear) entanglement molecular weight for the KG model, so the quantities reported here are only apparent or crossover scaling exponents. Nevertheless, the exponent values and trends will prove insightful in understanding the effect of the mechanical bond on ring conformations. The m-dependent apparent scaling exponents, $\nu_{g,r}(m)$ and $\nu_d(m)$, are calculated from $R_{g,r}^2$ and R_d^2, respectively, by finite difference, and are presented in Table 1 for various ring topologies. Free rings scale nearly ideally at small m, with exponents decreasing modestly as m increases, consistent with other simulations of ring polymer melts.[35,38,41−43,77] For the threaded rings, the scaling exponents also decrease as m increases, but the values

https://dx.doi.org/10.1021/acs.macromol.9b02706
Macromolecules 2020, 53, 3390−3408

are much smaller overall, as low as 0.37 for the largest ring sizes. These results lead to an apparent "paradox": such small scaling exponents typically indicate topological compression of rings, leading to smaller polymers, but the mechanical bonds actually expand the rings (Table 1). Perhaps the unusually small scaling exponents arise because the dimensions of the threaded rings are converging toward those of the unthreaded ones as m increases; this convergence would naturally lead to smaller apparent scaling exponents. Indeed, the results shown in Table 1 indicate that rings tend to become more ideal as m increases for all topologies (i.e., number of threadings). This picture is also supported by the density profiles in Figure 3: the qualitative differences between the profiles of chain centers and free rings are considerably reduced at large ring sizes. However, this does not appear to be the case in dilute solution conditions as revealed by recent Monte Carlo simulations of linked and unlinked rings, which do not exhibit the "paradox" mentioned above. Indeed, linked rings are still considerably larger than unlinked ones in dilute solution conditions, even for very large polymers,[78] and show nearly identical scaling behavior.[75,78,79] The primary difference between these two scenarios is the presence of intermolecular (interchain) interactions. These observations suggest an interplay of two effects in poly[n]-catenane melts: the mechanical bonds increase the ring size and change the ring shape (Table 1), thus altering the *inter* molecular interactions with other rings in the melt, affecting the scaling of the ring size with increasing m. In summary, ring dimensions in poly[n]catenanes appear to be significantly affected by both the mechanical bonds and the intermolecular interactions.

Thus far, only the overall size and shape of the rings have been considered; now the specific conformations of the macrocycles are studied. These conformations may be quantitatively analyzed in terms of the Rouse modes, which are essentially Fourier modes of the chain.[72] For ring polymers,[71] these modes are written:

$$\boldsymbol{X}_q = \sum_{i=1}^{m} \boldsymbol{R}_i \cos\left(\frac{\pi q i}{m}\right) \tag{6}$$

where $\boldsymbol{R}_i$ is the position of bead i, and q is the mode number. For ring polymers, only even mode numbers q are allowed. These modes are associated with a set of eigenvalues:

$$\lambda_q = 4 \sin^2\left(\frac{q\pi}{2m}\right) \tag{7}$$

The mean-squared mode amplitudes $\langle X_q^2 \rangle$ contain information about the conformation of the polymer at length scales of m/q along the chain contour, and their sum is proportional to $R_{g,r}^2$. When scaled by the eigenvalues, the amplitudes represents effective bond lengths (squared) at the corresponding length scale. For ideal Gaussian chains, these bond lengths are constant for all length scales; in reality, the bond lengths typically increase toward a plateau at large length scales (m/q) because of local chain stiffness effects. These effective bond lengths are plotted as a function of length scale in Figure 4 for all ring sizes and topologies (sets of curves for different m have been shifted vertically for clarity). At the longest length scales, the rings are expanded by the mechanical bonds, in agreement with the previously discussed results on ring dimensions. However, at all shorter length scales, the mode amplitudes for the threaded macrocycles are smaller than those of the free rings, indicating that the mechanical bond effectively

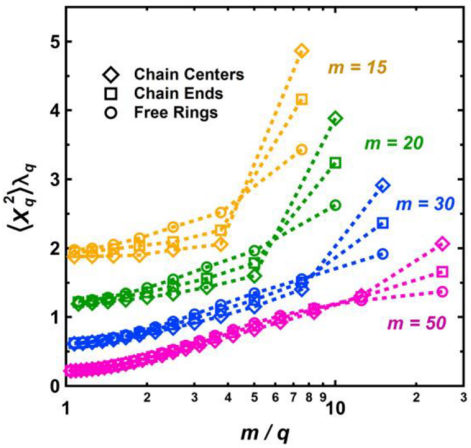

Figure 4. Mean squared amplitudes of the Rouse modes for rings (eq 6) within poly[n]catenanes. Sets of curves for each m have been shifted vertically for clarity.

compresses the segments locally compared to free rings, with doubly threaded rings being the most affected. As is the case for other structural properties, the size of these effects is diminished as m increases. Since these two effects were also observed in dilute solution conditions,[68] they are likely related to the mechanical bonds alone, rather than intermolecular interactions.

The single-ring structure factor also shows some signatures of the mechanical bond. The single ring structure factor is defined as

$$S(k) = \frac{1}{m}\left\langle \sum_{i,j=1}^{m} \frac{\sin k r_{ij}}{k r_{ij}} \right\rangle \tag{8}$$

where r_{ij} is the distance between beads i and j within the same ring, and the angled brackets denote an ensemble average over all rings of the same topology, that is, all chain center or chain end macrocycles in poly[n]catenanes, or all rings in ring polymer melts. This function provides information on polymer conformation and statistics in reciprocal space and can be obtained experimentally via neutron scattering. As expected, all systems show a Guinier regime at low-k and peaks at high-k, the latter being caused by the covalent connectivity between beads. However, for threaded rings, the structure factor also exhibits a pronounced shoulder at $kR_{g,r} \approx 4$, as shown in Figure 5a. This feature appears at the same value of $kR_{g,r}$ for all ring sizes, indicating that it is not caused by bead connectivity but is instead related to the structure of rings at the segmental level. This shoulder is absent for free rings, as shown in Figure 5b, indicating that it is a feature unique to the mechanical bond. As with other features, the size of the effect is reduced as m is increased. This distinctive feature may be related to the peaked density profiles seen in Figure 3. However, the connection between the two observations is not entirely clear. For instance, free rings also show a maximum in the density profile for m = 15, but this system does not show any additional shoulder in the structure factor. Furthermore, the position of the peak in the density shifts to lower values of $r/R_{g,r}$ as m is increased, while the position of the peak/shoulder in the structure factor is virtually constant for all m. Ultimately, these two quantities probe the structure in different ways, so no immediate connection between them is available.

https://dx.doi.org/10.1021/acs.macromol.9b02706
Macromolecules 2020, 53, 3390−3408

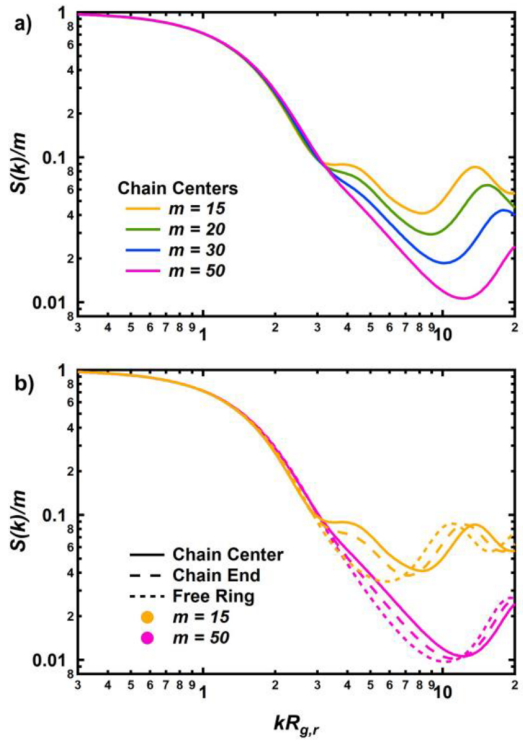

Figure 5. (a) Chain center single-ring structure factor for various m. (b) Structure factor for all ring topologies for smallest and largest m values. Note that the k-values have been scaled by the radius of gyration of each ring. These data were taken from systems with $n = 7$ but are in quantitative agreement with other values of n.

5. CHAIN CONFORMATION

As poly[n]catenanes have an overall linear structure, their properties can be conveniently studied by coarse-graining them into simple linear polymers. Following previous work,[68] each ring is defined as an effective monomer with its position given by the ring center-of-mass; the conformations of the chains are examined in terms of these effective monomers. First, structural properties that do not depend on chain length, n, are considered; among these are the mechanical bond lengths at the chain end, b_e, and chain center, b_c, defined as the separation distance between ring centers-of-mass at these points in the chain. These quantities are shown in Table 2; since they have essentially no dependence on n (see Appendix A, Figure A1b), they are calculated from the systems with $n = 25$ for simplicity. The bond lengths are somewhat smaller at the chain ends compared to chain centers, consistent with the previous observation that the rings are smaller at the chain ends (Table 1). One would expect that these bond lengths scale with m in a manner similar to the ring size ($R_{g,r}$ or R_d). Although these apparent scaling exponents, ν_b, are indeed in the range 0.4−0.5 for the chain center bonds (Table 2), the exponents actually increase with m, in contrast to the ring size scaling exponents, which decrease with m (Table 1). The reason for this discrepancy is unclear but may be related to the interplay of the mechanical bonds and intermolecular interactions mentioned in the previous section; further study is required to clarify the situation.

The effective bond length, b_{eff}, measures the polymer stiffness and is defined in terms of the end-to-end distance as $R_e^2 = (n-1)b_{\text{eff}}^2$; note that R_e^2 is the mean-squared distance between the centers-of-mass of the chain-end macrocycles and will be discussed later. Consistent with the results of Wittmer et al.,[80,81] the quantity $R_e^2/(n-1)$ depends linearly on $1/\sqrt{n}$, so a simple linear regression can be used to estimate b_{eff}^2 in the asymptotic limit ($n \to \infty$); these data and their apparent scaling exponents with m, denoted $\nu_{b,\text{eff}}$, are shown in Table 2. As expected, the effective bond lengths increase with m, reflecting the larger size of the elementary macrocycles. Similar to the mean bond lengths discussed above, the apparent scaling exponents of effective bond lengths increase with m. However, the actual values of the exponents are considerably smaller: in the range of 0.29−0.34. Essentially, the effective bond lengths increase with m more slowly that the true bond lengths. The ratio of these two values, b_{eff}/b_c is simply the square root of the characteristic ratio and therefore measures the effective stiffness of the polymer; this value (also shown in Table 2) decreases with m, indicating that poly[n]catenanes with larger rings are more flexible, in a relative sense. This result agrees with our previous work on isolated chains.[68] Finally, the persistence length is calculated in two ways: (1) direct calculation using the polymer radius of gyration[82] and subsequent normalization by b_c, and (2) by fitting the bond vector orientational correlation function to an exponential decay. The first method includes information about all beads within the polymer since R_g is calculated using every bead; the second method only accounts for interactions at the macrocycle center-of-mass level. Because of this, the numerical values are quite different. In general, these two measures of persistence length do not agree with each other for "thick" macromolecules,[83−85] so the result is not surprising. Nevertheless, both measures of persistence length follow the same trend as the normalized effective bond lengths: larger rings lead to more flexible poly[n]catenanes.

The observations above can be explained qualitatively with a simple excluded volume argument. Because the melt has finite compressibility, segments (i.e., rings) within the same polymer chain repel each other at short distances due to unscreened excluded volume. In turn, this excluded volume should be

Table 2. Structural Properties of Poly[n]catenanes[a]

m	b_c	ν_b	b_e	b_{eff}	$\nu_{b,\text{eff}}$	b_{eff}/b_c	l_p^g	l_p^e	n_e
15	1.98		1.75	3.24		1.64	1.48	1.12	43
20	2.23	0.41	2.01	3.52	0.29	1.58	1.38	1.01	45
30	2.69	0.46	2.47	4.02	0.33	1.49	1.23	0.84	45
50	3.46	0.49	3.23	4.79	0.34	1.38	1.07	0.66	42

[a]Intrinsic structural properties of poly[n]catenanes: chain center bond length (b_c), apparent scaling of b_c with m (ν_b, calculated by finite difference), chain end bond length (b_e), effective bond length (b_{eff}), apparent scaling of b_{eff} with m ($\nu_{b,\text{eff}}$, calculated by finite difference) and normalized effective bond length (b_{eff}/b_c), persistence length from radius of gyration (l_p^g), persistence length from bond vector correlations (l_p^e), estimated entanglement length (n_e, see Section 6 for details and discussion). See main text for additional details.

https://dx.doi.org/10.1021/acs.macromol.9b02706
Macromolecules 2020, 53, 3390−3408

related to the local bead density within the segments. For poly[n]catenane macrocycles, this bead density decreases as m increases; this is true for any molecule that is not completely globular, that is, $R \sim N^{1/3}$. Therefore, poly[n]catenanes with larger rings experience less intrachain repulsion between macrocycles, which makes the chains more flexible compared to those with smaller rings. Of course, the rings will also exhibit some topological excluded volume,[51] which is expected to grow with m,[86] but such effects should be negligible compared to the molecular (bead) excluded volume for the small rings considered here.

The apparent scaling of poly[n]catenane size with n depends strongly on the particular measure: end-to-end distance, R_e, or radius of gyration, R_g. The former is calculated as the distance between the centers-of-mass of the chain-end macrocycles, while the latter includes contributions from all beads in the system. In Appendix B, it is shown that the two quantities may be estimated in terms of the radius of gyration of the rings, $R_{g,r}$, and the effective bond length, b_{eff}, by the relations:

$$R_e^{\,2} = (n-1)b_{\mathrm{eff}}^{\,2} \approx nb_{\mathrm{eff}}^{\,2} \tag{9}$$

$$R_g^{\,2} \approx \frac{nb_{\mathrm{eff}}^{\,2}}{6} + R_{g,r}^{\,2} + \frac{b_{\mathrm{eff}}^{\,2}}{6n} \tag{10}$$

Note that quantitative agreement with eqs 9 and 10 is not expected as a variety of approximations have been employed. Nevertheless, the same qualitative trends should be apparent in simulation data. For large values of n, eqs 9 and 10 indicate that both R_e and R_g approach ideal scaling, $R_e \sim R_g \sim n^{1/2}$; this result is confirmed in Figure 6 for all poly[n]catenane systems.

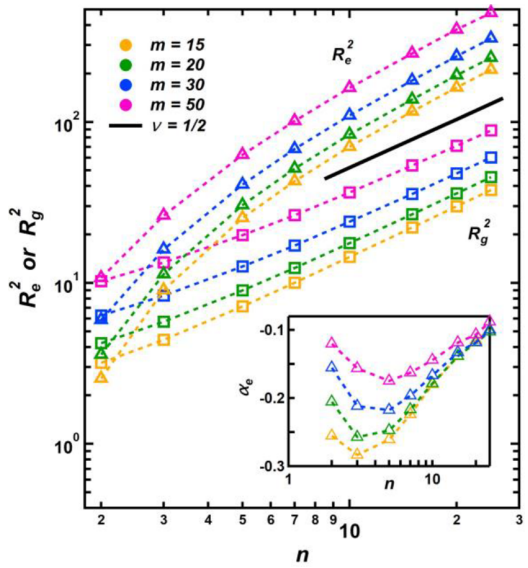

Figure 6. Mean-squared end-to-end distance and radius of gyration for poly[n]catenanes as a function of the number of rings per chain. Inset: non-Gaussian parameter for the distribution of end-to-end distances.

Furthermore, the distribution of end-to-end vectors becomes more Gaussian (ideal) for large n as determined by a non-Gaussian parameter similar to eq 5 (Figure 6 inset). These results demonstrate that poly[n]catenanes are similar to linear polymers at long length scales. The fact that the ratio $R_e^{\,2}/R_g^{\,2}$ is nearly equal to the ideal chain value of six at large n further supports this conclusion. However, the apparent exponents of R_e and R_g in the low-n crossover regime approach the ideal limit from different directions, as shown in Figure 7 (calculated

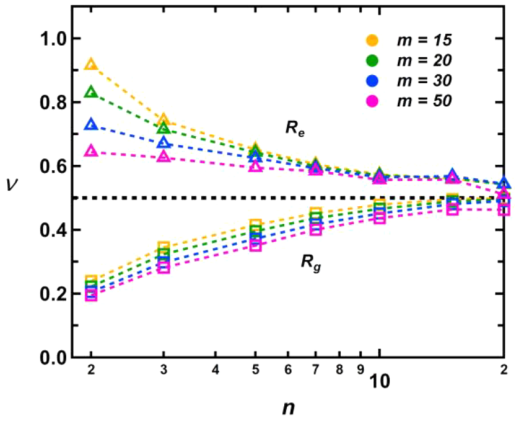

Figure 7. n-dependent apparent scaling exponents, ν, for end-to-end distance, R_e, and radius of gyration, R_g, of poly[n]catenanes calculated by finite difference. The dashed black line indicates the ideal (Gaussian) limit.

by finite difference). The apparent scaling exponents of R_e are much larger than 1/2 at small n and slowly decrease toward the ideal value, while the apparent scaling exponents of R_g are considerably lower than 1/2 at small n, with values as small as 0.2 observed for the largest ring sizes. The rapid apparent scaling of R_e is typical for linear polymers and is caused by local stiffness of the chain and unscreened excluded volume effects. On the other hand, the apparent scaling of R_g is quite unusual: such exceptionally small exponents indicate highly compact conformations which slowly relax to ideal coils at large n. This result can be understood in terms of eq 10, which contains three terms: an ideal chain contribution (first term), an additive correction that is independent of n (second term), and a higher order correction that decays quickly with n (third term), which can be neglected in the present analysis. The second term arises from the detailed local structure of the polymer, that is, the macrocycles, and causes reductions in the apparent scaling with n. In fact, from eq 10, the apparent scaling exponent can be approximated as $\nu \approx 1/2 - 3R_{g,r}^{\,2}/R_e^{\,2}$ (see Appendix B) so that corrections to the ideal chain value are related to the relative size of the macrocycles and the overall polymer. For larger rings or shorter chains, these corrections lead to smaller effective scaling exponents; both of these trends can be clearly seen in Figure 7. At large length scales, the details of the underlying ring structure become less important, and the poly[n]catenanes are dominated by their overall linear architecture, at which point the ideal scaling exponent of 1/2 is recovered.

The m-dependence of R_e and R_g can also be understood in terms of eqs 9 and 10. In particular, eq 9 indicates that R_e should depend on m only through the effective bond length, b_{eff} (neglecting chain end effects). The behavior in eq 10 is richer, as two m-dependent quantities are found: the effective bond length, b_{eff}, and the ring radius of gyration, $R_{g,r}$. As a result, no power-law behavior is expected except when the second and third terms of eq 10 can be ignored (i.e., for large n) or when both b_{eff} and $R_{g,r}$ have the same power-law dependence on m. However, the latter scenario is not observed

https://dx.doi.org/10.1021/acs.macromol.9b02706
Macromolecules 2020, 53, 3390−3408

in the simulation data as discussed above (cf. Tables 1 and 2): even for chain centers, $R_{g,r}$ increases considerably faster with m than does b_{eff}. As a result, the apparent scaling exponents of R_g with m systematically decrease with n from the free ring polymer values (roughly 1/2, see Table 1) at small n to the effective bond length values (roughly 1/3, see Table 2) at large n. In light of these observations, it is only useful to consider scaling behavior in the asymptotic limit of large n, where only the first term in eq 10 is important. In this scenario, R_e and R_g will have the same m-dependence, which, as mentioned above, enters through b_{eff}; this dependence was discussed above near the beginning of this section. To restate the main points, b_{eff} (and therefore R_e and R_g) grows very slowly with m owing to a reduction in effective chain stiffness. However, the rings studied here are not large enough to reach any asymptotic limit.

The shape of poly[n]catenanes can be characterized in more detail by the ratios of the gyration tensor eigenvalues, shown in Figure 8. For n = 2, these ratios are smallest, indicating a more

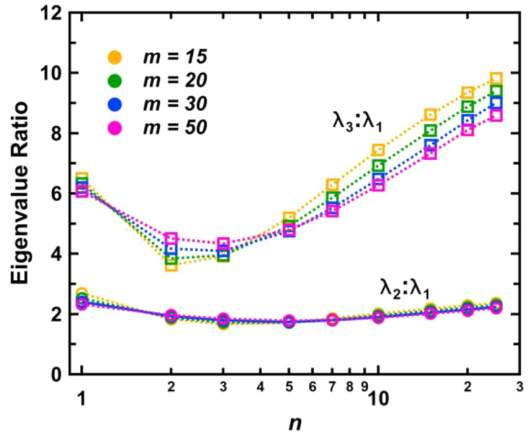

Figure 8. Ratio between average gyration tensor eigenvalues for poly[n]catenanes. The values for large n are close to the limiting values for linear polymers. However, the ratios for linear polymers approach this limit from above, rather than below.

spherical shape. At larger n, the ratios increase to values comparable to those of ordinary linear polymers ($\lambda_2/\lambda_1 \approx 2.6$, $\lambda_3/\lambda_1 \approx 10.7$),[2] suggesting a transition from globular to ideal coil conformations. Note that for linear polymers, the eigenvalue ratios are larger for smaller N because of local chain stiffness. In a similar manner, the ratios for n = 1 (i.e., ring polymers) are greater than those for n = 2.

Even at the largest values of n, poly[n]catenanes appear highly globular in the melt compared to dilute solution. A visualization of the molecule in the two contrasting conditions is shown in Figure 9. In good solvent conditions, the rings are expanded, along with the chain as a whole. However, once intermolecular effects are introduced in the melt, the polymer−polymer interactions compress the macromolecules drastically, transforming them into dense globule-like structures with just a few small protruding segments. These configurations are somewhat similar to those found in ring polymer melts, which is indeed expected since the lack of (covalent) chain ends in both systems requires that any interpenetrating segments must be loops.[37,38,43] Similar conformations involving segregated territories are also observed in cellular chromatin and imply considerable density inhomogeneities within single chains.[75,87] When the polymer is examined in terms of the ring COMs, the details of the globular structure are lost and the resulting linear polymer appears quite ordinary. Because of these observations, complex features are expected in the single-chain structure factor.

The single chain structure factor is calculated according to eq 8, except all pairs of beads on the same catenane (or linear chain) are included in the sum, and the average is taken over all chains in the system. For traditional linear polymers, the structure factors exhibit a large intermediate region where $S(k) \sim k^{-2}$ since polymers are statistically fractal objects, specifically ideal random walks in the melt.[88,89] At larger k, the structure factor oscillates because of local connectivity constraints at the bead level.[23] Meanwhile, for ring polymers, an additional region of $S(k) \sim k^{-3}$ has been observed at low-k for high-MW melts corresponding to a collapsed globule structure at large length scales.[38,90] For poly[n]catenanes, several distinct regions are observed, although they are narrow in wavevector range and therefore not well-developed, as shown in Figure 10. At low-k, the polymers exhibit a Guinier regime, as expected. At higher-k, a regime of ideal statistics with $S(k) \sim k^{-2}$ is expected for large n since the polymers are linear-like at large length scales, as previously discussed. However, no such regime is

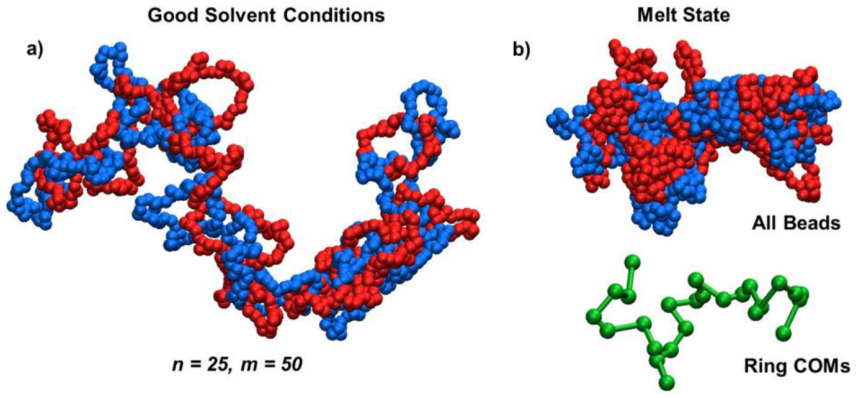

Figure 9. Visualizations of poly[n]catenanes with n = 25 and m = 50 in (a) good solvent conditions and (b) the melt state. Alternating rings are colored differently for visual clarity. Also shown in panel b are the ring COMs of the configuration (green) with the mechanical bonds represented by connections between the beads. The structure in the melt state shows several segregated territories, similar to those seen in nonconcatenated ring polymers and cellular chromatin.

https://dx.doi.org/10.1021/acs.macromol.9b02706
Macromolecules 2020, 53, 3390−3408

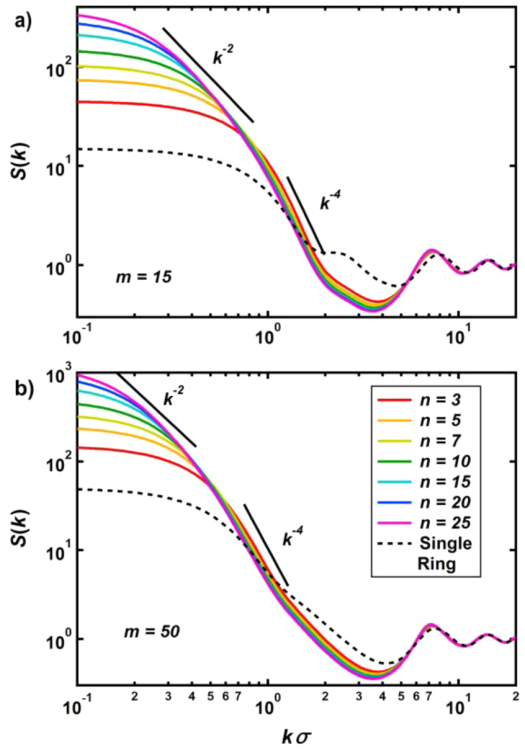

Figure 10. Single-chain structure factor for poly[n]catenanes of various n and (a) m = 15 or (b) m = 50. The dashed black curves show the single-ring structure factor for poly[n]catenane chain centers (cf. Figure 5a). The legend in panel b applies to both graphs.

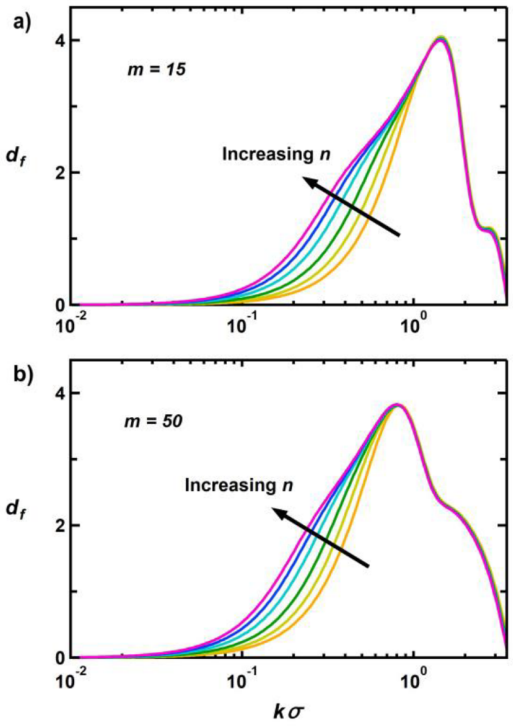

Figure 11. Differential fractal dimension for poly[n]catenanes of various n and (a) m = 15 or (b) m = 50. At low k-values (0.1−0.5), a small plateau develops in the neighborhood of d_f = 2, suggesting a slow approach toward ideal chain statistics.

easily distinguished in the structure factor. To more closely examine the behavior, it is helpful to study the differential apparent fractal dimension, defined as

$$d_f(k) = -\frac{d \log S(k)}{d \log k} \tag{11}$$

These functions are shown in Figure 11 for various systems. In the low-k range (∼0.1−0.5), the fractal dimensions exhibit a small shoulder in the neighborhood of d_f = 2, which slowly grows toward a quasi-plateau as n increases. Its value is consistent with Gaussian chain statistics, and the smallness of the regime suggests that the largest poly[n]catenanes are only just beginning to display ideal chain behavior.

Next a small apparent regime of $S(k) \sim k^{-4}$ is observed at intermediate k-values. This Porod-like behavior is typically associated with scattering from interfaces and other systems with density inhomogeneities. As we have pointed out above, poly[n]catenanes form segregated territories in the melt (Figure 9b), and the scattering from these regions (and their boundaries) may explain this regime. This will be discussed further below.

At even higher k-values, a third regime is observed with a power-law slope that depends on m, with smaller rings showing "flatter" curves in this region. This feature appears as a small shoulder in the differential fractal dimension, with the value of d_f depending strongly on m. For m = 15, this "shoulder" is actually a small peak. These features are strikingly similar to the signatures of the mechanical bond in the single-ring structure factor discussed in Section 4. In fact, both these features appear at the same k-values (see Figure 10), suggesting that they are the same phenomenon manifested in two different scattering functions. After this regime, the structure factor is dominated by local bead connectivity constraints.

To separate out the chain and ring structural contributions, the single polymer total intramolecular structure factor is computed at the coarse-grained level, considering only the macrocycle centers-of-mass as the scattering bodies. This function is compared to the full chain structure factor in Figure 12. At the coarsened resolution, the polymers are nearly ideal, and the structure factors agree quantitatively with the full structure factor at large length scales (low-k). However, most of the features in the higher-k regions are absent, indicating

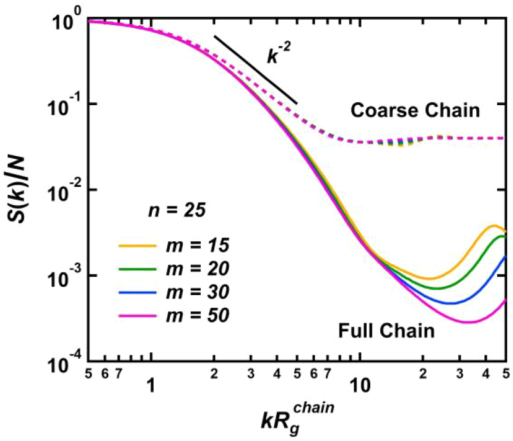

Figure 12. Single chain structure factor for poly[n]catenanes of various m at the coarse level compared with the fully detailed level.

https://dx.doi.org/10.1021/acs.macromol.9b02706
Macromolecules 2020, 53, 3390−3408

that all of these more unusual phenomena are intimately related to the underling structure of the rings. At high-k, the structure factor does oscillate very slightly (owing to the macrocycle connectivity), but this effect is very small and decays quickly.

Although the high-k regime can be easily interpreted as single-ring structure, the intermediate $S(k) \sim k^{-4}$ regime is quite unusual. Such scaling exponents are more typical of phase-separated systems in which the interface contributes strongly to the scattering.[91−93] However, the poly[n]catenanes considered here are neutral homopolymers, so there can be no phase separation in the ordinary sense. Nevertheless, such scaling implies density inhomogeneities along the chain, which are clearly visible in Figure 9b in the form of ring segments protruding from a globular-like core. To quantify these inhomogeneities, the average single-chain bead density is calculated as a function of the contour position using the following procedure. The ring center-of-mass positions of a given polymer are interpolated by a cubic spline function, and 20 equidistant points are placed between each center-of-mass. The local density of a single chain at a given point is then determined by the number of beads (in the same catenane) within a given distance of the point. Because each polymer is considered individually and only the single-chain densities are calculated, the resulting values may differ from the overall system density. To resolve differences in density at the appropriate length scales, the cutoff distance is taken to be one-half the radius-of-gyration of the chain-center macrocycles ($R_{g,r}$); other choices are also possible but give qualitatively similar results so long as the cutoff is not too large. These data are averaged over all polymers in the melt and multiple configurations for improved statistics. The resulting density profiles (denoted ρ_c) are shown as a function of contour position (denoted s) in Figure 13 for poly[n]catenanes with n = 10 and various m. For all m, these profiles show small but clear oscillations with a period of one mechanical bond in the chain contour space, indicating a "beads-on-a-string" structure. Interestingly, the maxima of the density occur at half-integer values of s, indicating that the highest densities are found at the "linked portion" of the macrocycles.[33] For the smallest rings, there is a smaller maximum found at whole integer values of s, which is likely caused by the threading segments being forced close to the ring center-of-mass by the small ring size; for larger m, this feature disappears. Different values of n yield quantitatively similar results. The length scale of the density oscillations in real space will be dominated by the separation of nearest-neighbor high-density regions. Since this separation is one mechanical bond in chain contour space, the separation in real space should be related to the mechanical bond length, b_c, and should therefore vary with m. If these oscillations cause the k^{-4} scaling in the structure factor, then the length scale of interest is determined by the position of the maximum in the differential fractal dimension: $d = 2\pi/k_{max}$. As expected, these length scales do in fact increase with m, and although they are considerably larger than the bond lengths, b_c, the ratio $d/b_c \approx 2.28$ is fairly constant for all ring sizes. These observations suggest that the unusually fast decay in the single-chain structure factor is related to the density variations associated with the linked portions of the macrocycles. Nevertheless, the quantitative differences in bond length and Porod-like length scales demand further study to better understand the territorial segregation observed in these polymers. In particular, it is not clear why the length scale d is so large, even larger than b_{eff}, so it is possible that there are multiple length scales associated with the density fluctuations in the polymers.

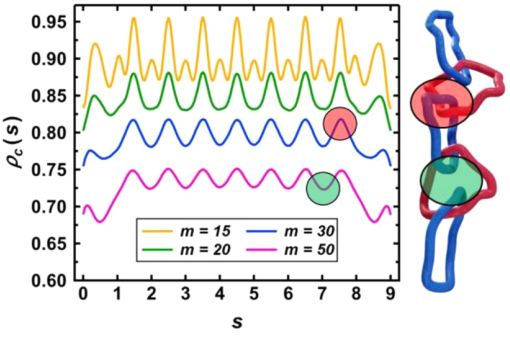

Figure 13. Single-chain density as a function of chain contour position for poly[n]catenanes of n = 10 and various m and companion illustration. See main text for details of the calculation. The maxima occur at approximately half-integer values of s, which correspond to the linked portions of the rings (red shaded areas), while the minima correspond to the chain centers (green shaded areas). For m = 15, the smaller maxima are caused by the close interaction of linked segments of next-nearest neighbor rings.

6. INTERMOLECULAR STRUCTURE

In the melt, high-MW linear and ring polymers interact strongly with neighboring chains, and these interactions can greatly affect both structure and dynamics. In particular, the interpolymer packing correlations are a functional of polymer conformation via the intramolecular structure factor examined in the previous section and the two functions are self-consistently coupled. Given the unusual intramolecular correlations studied earlier, it is expected that intermolecular structure may also show signatures of the complex poly[n]-catenane architecture. A key quantity is the intermolecular site−site correlation function, $g(r)$. Results are shown in Figure 14 for catenanes of n = 25 and various ring sizes. Like linear polymers, a pronounced correlation hole effect[88] is observed, which is nearly independent of ring size. For large n, the correlated part of $g(r)$ (defined as $h(r) = g(r) - 1$) exhibits an

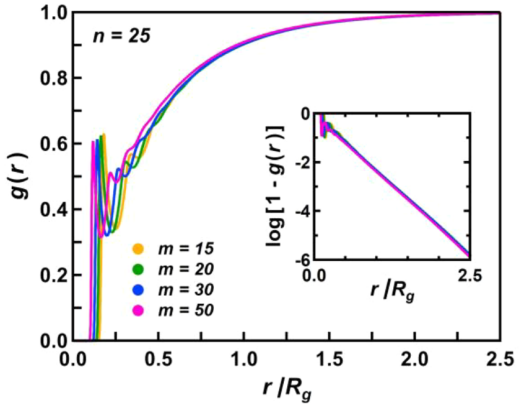

Figure 14. Intermolecular bead−bead correlation function for poly[n]catenanes of various m. Normalizing the distances by the polymer R_g results in collapse to a master curve for a given n. Inset: the logarithm of the nonrandom part of the correlation function. The linear dependence indicates exponential decay.

https://dx.doi.org/10.1021/acs.macromol.9b02706
Macromolecules 2020, 53, 3390−3408

exponential decay beyond very local length scales (Figure 14 inset), with a decay length of order the chain R_g. This feature is qualitatively the same as for melts of random coil chains; however, the form of the correlation for those systems is Yukawa, $h(r) \sim (1/r)\exp(-r/R_g)$. For a fixed value of m, the depth/width of the correlation hole increases with n as expected, as shown in Figure 15a. However, when normalized

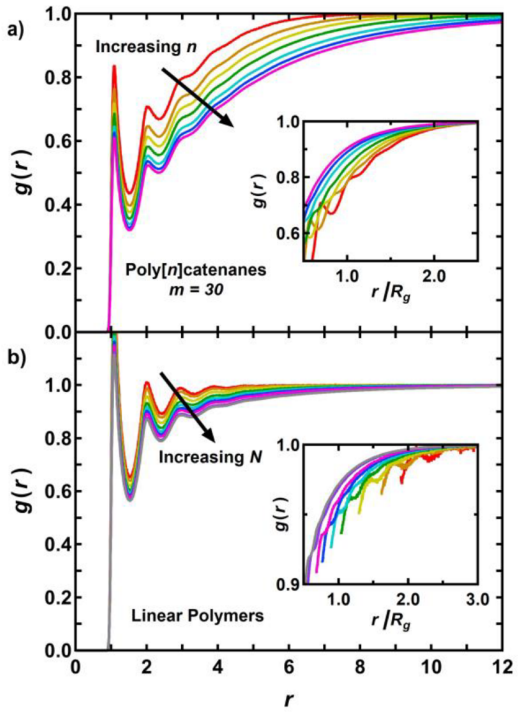

Figure 15. Intermolecular bead−bead correlation function for (a) poly[n]catenanes of m = 30 and variable n, and (b) linear polymers of variable N. The depth and width of the correlation hole effect increases with n and N, although the size of the effect is much larger for poly[n]catenanes. Inset: the same data with distance normalized by R_g. For clarity, only the data beyond the third solvation shell are displayed in the inset of panel b. The two systems are qualitatively similar, suggesting that poly[n]catenanes are comparable to linear polymers at long length scales.

by R_g, the width of the correlation hole actually decreases with n (Figure 15a inset), indicating that larger poly[n]catenanes exclude each other less strongly, similar to linear polymers (Figure 15b).

The dynamics of a tagged polymer in a dense liquid is often intimately related to the number of neighboring polymers it interacts with; this is true for linear chains, and ring polymers,[38] and is likely important for other complex architectures. Here, the number of neighbors, n_p, is calculated using both a direct and indirect method, which reveal different aspects of the interpenetrating melt structure. In the direct method, the intermolecular pair correlation function of the poly[n]catenane centers-of-mass is calculated and then integrated to a separation of R_g.[38] In the indirect method, the intermolecular site−site correlation function, $g(r)$, is integrated to R_g and then divided by N.[90] The direct method focuses on a coordination number at a coarse grained center-of-mass level in the spirit of polymers as soft particles, while the indirect method is the more local bead level analog. The results are shown in Figure 16. For linear polymers, the two

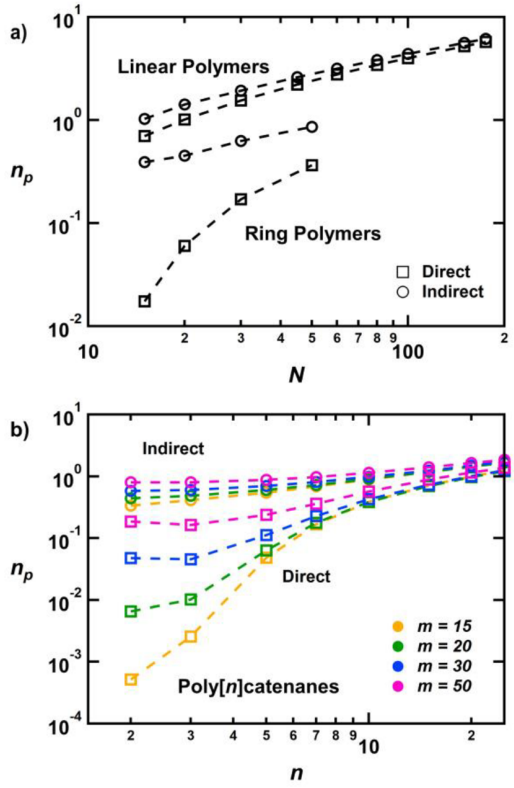

Figure 16. Average number of neighboring chains as calculated by the direct and indirect methods (see main text) for (a) linear and ring polymers as a function of N, and (b) poly[n]catenanes of various m as a function of n. Note that the scale bars for the two graphs are different: the poly[n]catenane values vary over a much larger range and are generally smaller than those of linear polymers.

methods give similar numerical values (Figure 16a), which scale nearly ideally with degree of polymerization, $n_p \sim N^{1/2}$. On the other hand, unlinked ring polymers have far fewer neighbors than linear chains, and the two methods disagree significantly, with the direct method giving values more than an order of magnitude smaller than the indirect one for small N. The small values of the direct method indicate that ring centers-of-mass cannot easily approach each other, while the larger values based on the indirect method reflect bead−bead contacts in the surface region of two partially overlapping macromolecules. This interpretation is supported by previous simulation results.[38,90] For poly[n]catenanes (Figure 16b), the indirect method yields $n_p \sim n^{1/2}$, as expected for ideal polymers. The quantitative values increase with as m increases, suggesting that larger rings allow for more interpenetration and more neighbors. However, for small n, the direct method gives values that are several orders of magnitude smaller, indicating that poly[n]catenane centers-of-mass cannot easily approach each other. The values do increase for larger m but are still far smaller than those of the indirect method. These results are qualitatively similar to those of unlinked ring polymers, indicating that short poly[n]catenanes primarily interact with their neighbors at the surface of the polymers and interpenetrate each other only weakly, consistent with the globular conformations at small n. At larger values of n, the results of the two methods approach each other, indicating a transition to more ideal chain behavior. For the KG model considered here, the entanglement length for linear chains is approx-

https://dx.doi.org/10.1021/acs.macromol.9b02706
Macromolecules 2020, 53, 3390−3408

imately $N_e \approx 85$,[26] at which point $n_p \approx 4$; this value is considerably larger than that of the longest poly[n]catenanes studied here, which have $n_p < 2$. As a result, it is unlikely that poly[n]catenanes of this length will be able to entangle in a meaningful way. Of course, the specific values reported in Figure 16 could be altered by adjusting the integration cut off for the two methods, but the same general trends are observed.

The density profiles of individual rings as a function of their distance from the overall polymer center of mass, also known as the self-densities, also provide information on polymer structure and interpenetration. The results for the smallest and largest poly[n]catenanes are shown in Figure 17 along with

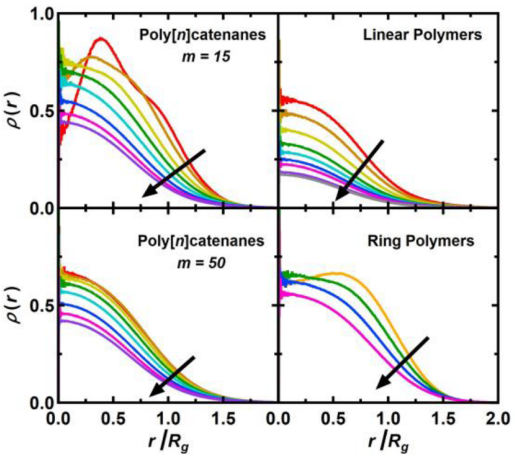

Figure 17. Single-chain bead density profiles as a function of distance from polymer center of mass for poly[n]catenanes with various m and n = 2−25 (left), compared with profiles for linear polymers of N = 15−175 and ring polymers of N = 15−50. The arrows indicate increasing molecular weight (n or N).

data for linear and ring polymers for comparison. For poly[n]catenanes with small rings, the profile shows distinct peaks/humps, which likely arise because of conformational restrictions imposed by the fluid structure, that is, the molecules are small enough that the solvation shells still influence the structure significantly; these features disappear as the molecular weights (and therefore polymer sizes) increase. For all ring sizes, as n increases, the density profiles become broader and the density at $r = 0$ decreases, indicating improved chain interpenetration. In general, the self-densities near $r = 0$ tend to be larger for poly[n]catenanes and ring polymers compared to linear chains. For ideal linear polymers, the self-density in this limit scales as $N^{-1/2}$, per the correlation hole effect. Figure 18a shows these data as a function of N for linear and ring polymers. The linear polymers obey ideal scaling, while the self-density of ring polymers is nearly independent of N, in agreement with previous simulations.[38] The same data for poly[n]catenanes are displayed in Figure 18b, which shows two distinct regimes. At small n, the self-density at the origin is nearly constant and quite large (note the total density is 0.85), similar to the behavior of ring polymers. In this region, the polymers strongly exclude their neighbors due to their globular shape, and interpenetration is limited. As n increases, the self-density then begins to decay according to the ideal scaling law $\sim n^{1/2}$, similar to linear polymers. The two regimes are quite sharply separated at $n = 10$, suggesting that there is a critical threshold above which poly[n]catenanes cross over from a

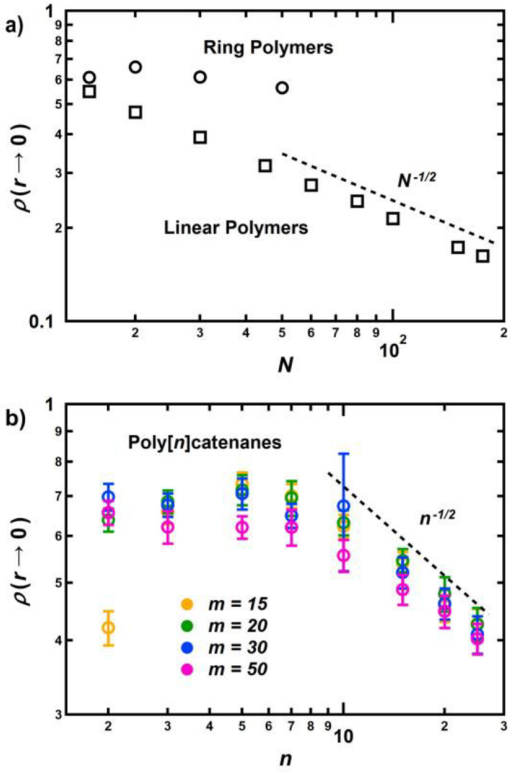

Figure 18. Single chain bead density at the polymer center of mass (also known as the self-density) for (a) linear and ring polymers as a function of N and (b) poly[n]catenanes of various m as a function of n. The dashed lines indicate the ideal linear polymer scaling laws. The error bars for the linear and ring polymer data are approximately the size of the data points and are therefore omitted for clarity. The wayward data point at $n = 2$ for $m = 15$ in panel b is caused by local bead packing effects.

globule-like conformation to an ideal chain conformation, although no such sharp transition is observed in the single-chain conformational properties (Section 5).

Finally, we consider the question of interchain entanglement of the polymers, which has important implications for the dynamics of these systems. For linear polymers, entanglements may be defined, identified, and quantified in many ways.[24−33] However, these methods cannot be directly applied to poly[n]catenanes since they do not have continuous (covalent) contours. Furthermore, any attempt to generate an equivalent linear polymer from a poly[n]catenane would necessarily lose information concerning local ring conformations. To keep the analysis simple, an estimate for the number of rings between entanglements, n_e, is calculated using the overlap parameter:

$$O = \frac{\rho {R_e}^3}{N} = \frac{\rho (n {b_{\text{eff}}}^2)^{3/2}}{nm} = \frac{\rho n^{1/2} {b_{\text{eff}}}^3}{m} \tag{12}$$

Linear polymers typically become entangled when $O \approx 10-20$; for instance, the linear polymers systems studied here have $N_e \approx 85$, which corresponds to $O \approx 18$. Therefore, n_e is estimated conservatively by setting $O = 10$ in eq 12 and solving for n. Of course, this analysis is highly simplified, as eq 12 is empirical and generally not applicable for cyclic or topologically complex polymers. Nevertheless, it provides a useful starting point for studying the entanglement properties of these polymers as their overall architecture is linear at long length scales and

https://dx.doi.org/10.1021/acs.macromol.9b02706
Macromolecules 2020, 53, 3390−3408

interchain entanglement is fundamentally a large-length scale phenomenon. The results of the calculation are shown in Table 2. The values are all roughly $n_e \approx 45$, independent of m, and much larger than the longest chains studied ($n = 25$). The large estimates of n_e agree well with the earlier observation that these polymers and their rings do not interpenetrate each other strongly. The lack of dependence on m is somewhat unexpected since an idealized poly[n]catenane would have an effective bond length proportional to ring size $b_{\text{eff}} \sim m^{1/2}$ and therefore $n_e \sim m^{-1}$ by eq 12. However, as discussed previously, the effective bond lengths grow slowly with m, leading to greater relative flexibility and therefore modifying the scaling of n_e with ring size. On the basis of these results, interchain entanglement should not affect the dynamics of the poly[n]catenanes studied here, which will be discussed in a later publication.

7. CONCLUSIONS

The static properties of poly[n]catenane melts have been systematically studied by molecular dynamics simulations and the key features that distinguish these unusual polymers from their linear (and cyclic) counterparts identified. The mechanical bonds significantly perturb the thermodynamics of the system, with large deviations in pressure observed as a consequence of the topological attraction between linked rings. These same mechanical bonds alter the conformations of the rings within catenanes and lead to nontrivial scaling with ring size. The polymers possess complicated intramolecular scattering functions that exhibit many more features than linear polymers, including unusual scaling relationships, which can be attributed to density inhomogeneities along the poly[n]catenane chain contour arising from the mechanical bonds and intermolecular topological effects. For relatively small degrees of polymerization, the poly[n]catenanes are highly globular and interact with their neighbors only at the surface of the polymer. As the number of rings increases, the conformations of poly[n]catenanes begin to resemble those of ideal chains with the number of neighboring chains following the expected scaling.

For the current synthetically accessible chain lengths studied here ($n < 25$), there is no indication that interchain entanglement plays a significant role. In fact, the large n_e values of poly[n]catenanes may explain some of the properties observed experimentally.[66] In particular, these polymers form powders, while chemically similar linear polymers of comparable molecular weight, can be processed into stable films. This difference may be caused by the intermolecular interactions: these molecules contain many rigid aromatic groups (necessary for the metal-templating synthesis), which can result in pervasive $\pi-\pi$ stacking interactions between the polymers. Such interactions are probably somewhat inhibited by the interlocking structure, reducing the cohesive energy density. However, based on the results presented here, interchain entanglement is likely also a factor. Since linear polymers entangle at much lower molecular weights than poly[n]catenanes, the stable films obtained experimentally from linear polymers of similar chemistries are likely entangled, improving stability below the glass transition temperature. Experimental linear poly[n]catenanes prepared to date have average degrees of polymerization (n) of 10−15, far too small to entangle according to our simulations, which suggest that at least an n of 45 is required to access poly[n]catenane materials suitable for rheological testing. Note, however, that the model poly[n]catenanes studied here are composed of fully flexible segments with no complex chemical motifs present, so the results here may not be immediately applicable to synthetically realizable systems. More generally, the results presented here suggest that macrocycle size is a key design parameter for poly[n]catenane systems. The ring size not only influences the polymer contour length but also alters its flexibility and may enhance or inhibit interchain entanglement at large n. More interestingly, catenanes are typically stimuli-responsive moieties, with dynamical motions that may be switched on or off by the appropriate stimulus,[55] and poly[n]catenanes are no exception.[66] The ring size will control the length scale associated with such switching behavior and how its effects are propagated along the chain.

APPENDIX A: SYSTEM PREPARATION

Because of very long relaxation times, simulations of high-MW linear polymers require sophisticated techniques for efficient and proper equilibration.[94−97] Unfortunately, many of these methods allow for chain crossings or otherwise alter the molecular topology and therefore cannot be applied to poly[n]catenanes; brute force equilibration must therefore be used. The systems studied here were prepared by a multistep process:

(a) A single, isolated poly[n]catenane was constructed as in previous work[68] and simulated for $5 \times 10^5 \tau$ to achieve an equilibrium conformation. Note that this time period is many-times the longest relaxation time of the isolated molecule (even for the largest n and m values).
(b) The molecule was duplicated and placed with random orientation at the vertices of a large cubic lattice while ensuring that no two molecules were overlapping.
(c) The system was evolved according to the production parameters given in the main text under the additional influence of a Berendsen barostat[98] with a time constant of 2τ and a pressure of 5 ε/σ^3 to compress it while recording particle coordinates periodically.
(d) A configuration with density close to the target value was selected, and box dimensions were adjusted to precisely match the desired density.
(e) The system was equilibrated for 10^6-10^7 τ, depending on its size (see Table A1 for details, "Equilibration #1").

Table A1. Poly[n]catenane System Details[a]

N	n	m	equilibration #1 (τ)	equilibration #2 (τ)	production (τ)
500	1	15,20,30,50	10^6	10^6	10^6
250	2	15,20,30,50	10^6	10^6	10^6
250	3	15,20,30,50	10^6	10^6	10^6
200	5	15,20,30,50	10^6	10^6	10^6
200	7	15,20,30,50	10^6	10^6	10^6
200	10	15,20,30	10^6	10^6	10^6
200	10	50	5×10^6	10^6	5×10^6
150	15	15,20,30	5×10^6	10^6	2×10^6
150	15	50	5×10^6	10^6	5×10^6
100	20	15,20,30	5×10^6	10^6	3.5×10^6
100	20	50	5×10^6	2.5×10^6	5×10^6
100	25	15,20,30	5×10^6	10^6	5×10^6
100	25	50	10^7	2.5×10^6	10^7

[a]Summary of poly[n]catenane systems studied and the equilibration/production simulation times.

https://dx.doi.org/10.1021/acs.macromol.9b02706
Macromolecules 2020, 53, 3390−3408

(f) To generate independent realizations for statistical analysis, the final configuration from Step e was given new particle velocities (drawn from a Boltzmann distribution) and evolved for an additional 10^6 −5 × 10^6 τ, depending on the system size (Table A1, "Equilibration #2"). The process was repeated to generate five independent realizations of the system. The resulting configurations were used as the starting points for production simulations.

After this procedure, the systems are well-equilibrated by several common measures. During Step e above, it is observed that the poly[n]catenane center-of-mass mean-squared-displacement reaches values several-times larger than the polymer size and that the average end-to-end vector autocorrelation function completely decays well before the end of the equilibration period (note that the end-to-end vector is defined by the centers-of-mass of the chain end macrocycles as discussed in the main text). Furthermore, both equilibration periods are much longer than the longest relaxation times of the polymers, which will be discussed in a future paper on dynamics.

Equilibration was also confirmed by examining polymer conformations directly. For linear polymer melts, the reduced mean squared internal distances are often used to assess equilibration:[95]

$$R^2(l)/l = \frac{\langle (\boldsymbol{R}_i - \boldsymbol{R}_{i+l})^2 \rangle}{l} \tag{A1}$$

where $\boldsymbol{R}_i$ is the position of monomer i on a given chain and the angled brackets indicate an ensemble average over all pairs of monomers separated by l bonds along the chain as well as all $\mathcal{N}$ chains in the system. This function increases smoothly with l to a plateau value which is roughly independent of N (and l) since linear polymers are approximately ideal in the melt. The values in eq A1 can be obtained directly from simulation trajectories and then used to assess system equilibration for any N. As the conformations of poly[n]catenanes are qualitatively similar to those of linear polymers at large length scales,[67−69] a similar measure may be employed for these systems. The function of eq A1 is modified by replacing the monomer position $\boldsymbol{R}_i$ with the position of the center-of-mass of ring i in the catenane. In analogy with linear polymers, this objective function should be independent of n and l for large l. Systems of long poly[n]catenanes are evaluated by comparing the mean squared internal distances to those of a slightly shorter polymers; n is built up gradually from n = 1 to 25, ensuring proper equilibration along the way. The reduced mean squared internal distances are shown in Figure A1a for poly[n]catenane systems with n > 3. The data are averaged over the final 10−50% of the first equilibration period (Step e, above). For each value of m, the data for all n and l are in excellent quantitative agreement, indicating well-equilibrated chain structures. At large l, the values decrease slightly, diverging from the apparent master curves. These deviations are caused by shortened mechanical bond lengths at the chain ends (Figure A1b). The chain ends contribute more strongly to eq A1 at larger l, thus lowering the reduced internal distances. In Figure A1a and b, the data sets achieve plateau values at large distances. These plateau values are related to the squared effective bond length, b_{eff}^2, and the central bond length, b_c, of the polymers (Table 2), respectively, and are discussed in Section 5.

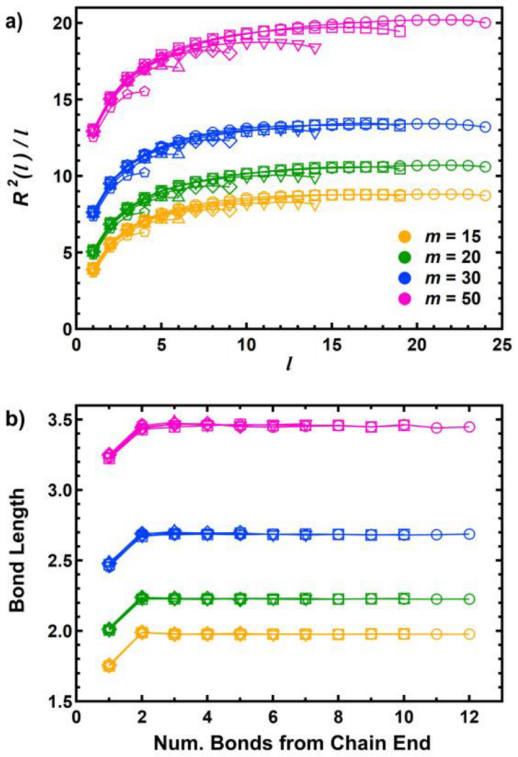

Figure A1. (a) Reduced mean-squared internal distances for poly[n]catenanes of various ring sizes, m (eq A1). (b) Mechanical bond length as a function of the number of bonds away from the catenane chain end. The different symbols indicate different values of n: 5 (pentagons), 7 (triangles), 10 (diamonds), 15 (downward triangles), 20 (squares), and 25 (circles).

Linear polymer systems were equilibrated by the DPD push off method,[96] followed by an additional equilibration period of 10^6 τ. To generate independent samples for statistical analysis, the particles were given new velocities and equilibrated for a further 10^6 τ to generate five independent realizations of each system to use as starting points for production simulations. See Table A2 for details of the linear systems studied in this work. Eq A1 was used to validate the systems, and the results agree quantitatively with the existing literature.[95]

Table A2. Linear Polymer System Details[a]

$\mathcal{N}$	N	production (τ)
500	15	10^6
500	20	10^6
500	30	10^6
500	45	10^6
500	60	10^6
500	80	10^6
500	100	10^6
500	150	3 × 10^6
500	175	5 × 10^6

[a]Summary of linear polymer systems studied and the production simulation times.

https://dx.doi.org/10.1021/acs.macromol.9b02706
Macromolecules 2020, 53, 3390−3408

APPENDIX B: POLY[N]CATENANE DIMENSIONS

The mean-squared radius of gyration of a poly[n]catenane can be calculated from the average distance between all pairs of beads in the polymer according to the formula:

$$R_g^2 = \frac{1}{2N^2}\sum_{i,j=1}^{N}\langle x_{ij}^2\rangle \tag{B1}$$

where $N = nm$, and $\langle x_{ij}^2\rangle$ is the mean-squared distance between beads i and j. R_g^2 is therefore calculated by evaluating each of the terms in the symmetric $N \times N$ matrix $\langle x_{ij}^2\rangle$. It is convenient to break up this matrix into blocks of size $m \times m$ such that the diagonal blocks represent the distances between beads on the same ring and off-diagonal ones represent the distances between beads on different rings. Making the approximation that all n rings are statistically identical and ignoring chain end effects, eq B1 can be rewritten as

$$R_g^2 \approx \frac{1}{2N^2}\left[n\sum_{i,j=1}^{m}\langle x_{\alpha i,\alpha j}^2\rangle + \sum_{k=1}^{n-1}2(n-k)\sum_{i,j=1}^{m}\langle x_{\alpha i,(\alpha+k)j}^2\rangle\right] \tag{B2}$$

where $\langle x_{\alpha i,\beta j}^2\rangle$ represents the mean-squared distance between bead i on ring α and bead j on ring β. The first term in brackets represents the diagonal blocks of the matrix $\langle x_{ij}^2\rangle$, while the second term represents the off-diagonal ones. The diagonal blocks are evaluated directly using eq B1 applied to individual macrocycles:

$$R_{g,r}^2 = \frac{1}{2m^2}\sum_{i,j=1}^{m}\langle x_{\alpha i,\alpha j}^2\rangle \tag{B3}$$

By rearranging eq B3 and substituting into the first term in brackets in eq B2, one finds:

$$R_g^2 \approx \frac{1}{2N^2}\left[2nm^2R_{g,r}^2 + \sum_{k=1}^{n-1}2(n-k)\sum_{i,j=1}^{m}\langle x_{\alpha i,(\alpha+k)j}^2\rangle\right] \tag{B4}$$

The off-diagonal components (second term in brackets in eq B4) can also be computed under certain approximations. To do so, $\langle x_{\alpha i,\beta j}^2\rangle$ is expressed as the sum of a series of vectors:

$$\langle x_{\alpha i,\beta j}^2\rangle = \langle[(\boldsymbol{R}_{\alpha i} - \boldsymbol{R}_{\alpha,\mathrm{cm}}) + (\boldsymbol{R}_{\alpha,\mathrm{cm}} - \boldsymbol{R}_{\beta,\mathrm{cm}}) - (\boldsymbol{R}_{\beta j} - \boldsymbol{R}_{\beta,\mathrm{cm}})]^2\rangle \tag{B5}$$

where $\boldsymbol{R}_{\alpha i}$ is the position of bead i on ring α, and $\boldsymbol{R}_{\alpha,\mathrm{cm}}$ is the position of the center-of-mass of ring α. The three vectors in eq B5 are approximated as statistically independent, which is not the case for neighboring (i.e., linked) rings especially at small m but should be fairly accurate for separations greater than the Kuhn length and therefore suffice for a first approximation. Expanding the square and evaluating the average, all cross terms disappear:

$$\langle x_{\alpha i,\beta j}^2\rangle \approx \langle(\boldsymbol{R}_{\alpha i} - \boldsymbol{R}_{\alpha,\mathrm{cm}})^2 + (\boldsymbol{R}_{\alpha,\mathrm{cm}} - \boldsymbol{R}_{\beta,\mathrm{cm}})^2 - (\boldsymbol{R}_{\beta j} - \boldsymbol{R}_{\beta,\mathrm{cm}})^2\rangle \tag{B6}$$

It is now helpful to recall that the radius of gyration of a polymer of N segments can also be expressed as the average mean squared distance between each particle and the polymer center-of-mass, denoted $\boldsymbol{R}_{\mathrm{cm}}$:

$$R_g^2 = \frac{1}{N}\sum_{i=1}^{N}\langle(\boldsymbol{R}_i - \boldsymbol{R}_{\mathrm{cm}})^2\rangle \tag{B7}$$

By summing eq 6 over all i and j, substituting Eq B7 and assuming Gaussian statistics for the ring center of mass separations, we find:

$$\sum_{i,j=1}^{m}\langle x_{\alpha i,\beta j}^2\rangle \approx 2m^2R_{g,r}^2 + m^2|\beta-\alpha|b_{\mathrm{eff}}^2 \tag{B8}$$

This expression is substituted into eq B4 to obtain

$$R_g^2 = \frac{1}{2N^2}\left[2nm^2R_{g,r}^2 + \sum_{k=1}^{n-1}2(n-k)(2m^2R_{g,r}^2 + km^2b_{\mathrm{eff}}^2)\right] \tag{B9}$$

The sum may now be evaluated directly and the prefactor distributed among each of the terms. Making the substitution $N = nm$, the result reads:

$$R_g^2 = \frac{nb_{\mathrm{eff}}^2}{6} + R_{g,r}^2 + \frac{b_{\mathrm{eff}}^2}{6n} \tag{B10}$$

To estimate the effective scaling of eq B10 with n, the logarithmic derivative is calculated:

$$\nu = \frac{1}{2}\frac{d\log R_g^2}{d\log n} = \frac{n}{2R_g^2}\frac{dR_g^2}{dn} \tag{B11}$$

Evaluating eq B11 up to order n^{-1}, the result after some manipulation is

$$\nu = \frac{1}{2} - \frac{3R_{g,r}^2}{nb_{\mathrm{eff}}^2} \approx \frac{1}{2} - \frac{3R_{g,r}^2}{R_e^2} \tag{B12}$$

where $R_g^2 = (n-1)b_{\mathrm{eff}}^2$ is the end-to-end distance squared, defined as the mean squared distance between the centers-of-mass of chain end macrocycles. The latter follows from the assumption of Gaussian statistics for the ring center-of-mass separations invoked prior to eq B8.

AUTHOR INFORMATION

Corresponding Author

Juan J. de Pablo − *Pritzker School of Molecular Engineering, University of Chicago, Chicago, Illinois 60637, United States; Center for Molecular Engineering and Materials Science Division, Argonne National Laboratory, Lemont, Illinois 60439, United States;* orcid.org/0000-0002-3526-516X; Email: depablo@uchicago.edu

Authors

Phillip M. Rauscher − *Pritzker School of Molecular Engineering, University of Chicago, Chicago, Illinois 60637, United States*

Kenneth S. Schweizer − *Department of Materials Science, Materials Research Laboratory, Department of Chemical and Biomolecular Engineering, and Department of Chemistry, University of Illinois, Urbana, Illinois 61801-3028, United States*

Stuart J. Rowan − *Pritzker School of Molecular Engineering and Department of Chemistry, University of Chicago, Chicago, Illinois 60637, United States; Chemical and Engineering Sciences and Center for Molecular Engineering, Argonne National Laboratory, Lemont, Illinois 60439, United States;* orcid.org/0000-0001-8176-0594

Complete contact information is available at: https://pubs.acs.org/10.1021/acs.macromol.9b02706

https://dx.doi.org/10.1021/acs.macromol.9b02706
Macromolecules 2020, 53, 3390−3408

Notes

The authors declare no competing financial interest.

■ ACKNOWLEDGMENTS

The authors gratefully acknowledge Dr. Artem Rumyantsev, Prof. Michael A. Webb, Dr. Nicholas E. Jackson, and Cody T. Bezik for many helpful discussions. Special thanks to Dr. Rumyantsev for providing many insightful comments on an early version of this paper, and to Viviana Palacio-Betancur for the assistance with several figures. P.M.R. thanks the National Science Foundation (NSF) for the award of a Graduate Research Fellowship, Grant No. 1746045. Any opinions, findings, and conclusions or recommendations expressed in this material are those of the author(s) and do not necessarily reflect the views of the National Science Foundation. The theoretical and computational work presented here is supported by the Department of Energy, Office of Science, Basic Energy Sciences, Division of Materials Science and Engineering. Initial investigations of poly[*n*]catenane systems were also supported by the NSF under Grant Nos. CHE-1402849 and CHE-1903603. K.S.S. thanks the Pritzker School of Molecular Engineering for financial support during his sabbatical stay at the University of Chicago. The development of materials for impact mitigation, of which poly[*n*]catenanes represent a category, is supported by NIST through the Center for Hierarchical Materials Design (CHiMaD).

■ REFERENCES

(1) Doi, M.; Edwards, S. F. *The Theory of Polymer Dynamics*; Oxford University Press, 1986.
(2) Kremer, K.; Grest, G. S. Dynamics of entangled linear polymer melts: A molecular-dynamics simulation. *J. Chem. Phys.* **1990**, *92*, 5057−5086.
(3) Edwards, S. F. The statistical mechanics of polymerized material. *Proc. Phys. Soc., London* **1967**, *92*, 9−16.
(4) de Gennes, P. G. Reptation of a Polymer Chain in the Presence of Fixed Obstacles. *J. Chem. Phys.* **1971**, *55*, 572−579.
(5) Doi, M.; Edwards, S. F. Dynamics of concentrated polymer systems. Part 1.—Brownian motion in the equilibrium state. *J. Chem. Soc., Faraday Trans. 2* **1978**, *74*, 1789−1801.
(6) Doi, M.; Edwards, S. F. Dynamics of concentrated polymer systems. Part 2.—Molecular motion under flow. *J. Chem. Soc., Faraday Trans. 2* **1978**, *74*, 1802−1817.
(7) Doi, M.; Edwards, S. F. Dynamics of concentrated polymer systems. Part 3.—The constitutive equation. *J. Chem. Soc., Faraday Trans. 2* **1978**, *74*, 1818−1832.
(8) McLeish, T. C. B. Tube theory of entangled polymer dynamics. *Adv. Phys.* **2002**, *51*, 1379−1527.
(9) Edwards, S. F.; Vilgis, T. A. The tube model theory of rubber elasticity. *Rep. Prog. Phys.* **1988**, *51*, 243−297.
(10) Ball, R. C.; Doi, M.; Edwards, S. F.; Warner, M. Elasticity of entangled networks. *Polymer* **1981**, *22*, 1010−1018.
(11) Rubinstein, M.; Panyukov, S. Elasticity of Polymer Networks. *Macromolecules* **2002**, *35*, 6670−6686.
(12) Likhtman, A. E. Single-Chain Slip-Link Model of Entangled Polymers: Simultaneous Description of Neutron Spin-Echo, Rheology, and Diffusion. *Macromolecules* **2005**, *38*, 6128−6139.
(13) Ramírez-Hernández, A.; Peters, B. L.; Andreev, M.; Schieber, J. D.; de Pablo, J. J. A multichain polymer slip-spring model with fluctuating number of entanglements for linear and nonlinear rheology. *J. Chem. Phys.* **2015**, *143*, 243147.
(14) Sgouros, A. P.; Megariotis, G.; Theodorou, D. N. Slip-Spring Model for the Linear and Nonlinear Viscoelastic Properties of Molten Polyethylene Derived from Atomistic Simulations. *Macromolecules* **2017**, *50*, 4524−4541.
(15) Sussman, D. M.; Schweizer, K. S. Microscopic Theory of the Tube Confinement Potential for Liquids of Topologically Entangled Rigid Macromolecules. *Phys. Rev. Lett.* **2011**, *107*, 078102.
(16) Sussman, D. M.; Schweizer, K. S. Microscopic Theory of Entangled Polymer Melt Dynamics: Flexible Chains as Primitive-Path Random Walks and Supercoarse Grained Needles. *Phys. Rev. Lett.* **2012**, *109*, 168306.
(17) Sussman, D. M.; Schweizer, K. S. Entangled polymer chain melts: Orientation and deformation dependent tube confinement and interchain entanglement elasticity. *J. Chem. Phys.* **2013**, *139*, 234904.
(18) Dell, Z. E.; Schweizer, K. S. Segment-scale, force-level theory of mesoscopic dynamic localization and entropic elasticity in entangled chain polymer liquids. *J. Chem. Phys.* **2017**, *146*, 134901.
(19) Kirste, R. G.; Kruse, W. A.; Ibel, K. Determination of the conformation of polymers in the amorphous solid state and in concentrated solution by neutron diffraction. *Polymer* **1975**, *16*, 120−124.
(20) Lieser, G.; Fischer, E. W.; Ibel, K. Conformation of polyethylene molecules in the melt as revealed by small-angle neutron scattering. *J. Polym. Sci., Polym. Lett. Ed.* **1975**, *13*, 39−43.
(21) Benoit, H.; et al. Dimensions of a Flexible Polymer Chain in the Bulk and in Solution. *Nature, Phys. Sci.* **1973**, *245*, 13−15.
(22) Hsu, H.-P. Lattice Monte Carlo simulations of polymer melts. *J. Chem. Phys.* **2014**, *141*, 234901.
(23) Hsu, H.-P.; Kremer, K. Static and dynamic properties of large polymer melts in equilibrium. *J. Chem. Phys.* **2016**, *144*, 154907.
(24) Rubinstein, M.; Helfand, E. Statistics of the entanglement of polymers: Concentration effects. *J. Chem. Phys.* **1985**, *82*, 2477−2483.
(25) Kroger, M.; Ramırez, J.; Christian Ottinger, H. Projection from an atomistic chain contour to its primitive path. *Polymer* **2002**, *43*, 477−487.
(26) Everaers, R.; et al. Rheology and microscopic topology of entangled polymeric liquids. *Science* **2004**, *303*, 823−6.
(27) Zhou, Q.; Larson, R. G. Primitive Path Identification and Statistics in Molecular Dynamics Simulations of Entangled Polymer Melts. *Macromolecules* **2005**, *38*, 5761−5765.
(28) Shanbhag, S.; Larson, R. G. Chain Retraction Potential in a Fixed Entanglement Network. *Phys. Rev. Lett.* **2005**, *94*, 076001.
(29) Foteinopoulou, K.; Karayiannis, N. C.; Mavrantzas, V. G.; Kröger, M. Primitive Path Identification and Entanglement Statistics in Polymer Melts: Results from Direct Topological Analysis on Atomistic Polyethylene Models. *Macromolecules* **2006**, *39*, 4207−4216.
(30) Tzoumanekas, C.; Theodorou, D. N. Topological Analysis of Linear Polymer Melts: A Statistical Approach. *Macromolecules* **2006**, *39*, 4592−4604.
(31) Shanbhag, S.; Kröger, M. Primitive Path Networks Generated by Annealing and Geometrical Methods: Insights into Differences. *Macromolecules* **2007**, *40*, 2897−2903.
(32) Likhtman, A. E.; Ponmurugan, M. Microscopic Definition of Polymer Entanglements. *Macromolecules* **2014**, *47*, 1470−1481.
(33) Caraglio, M.; Micheletti, C.; Orlandini, E. Physical Links: defining and detecting inter-chain entanglement. *Sci. Rep.* **2017**, *7*, 1156.
(34) Cates, M. E.; Deutsch, J. M. Conjectures on the statistics of ring polymers. *J. Phys. (Paris)* **1986**, *47*, 2121−2128.
(35) Müller, M.; Wittmer, J. P.; Cates, M. E. Topological effects in ring polymers: A computer simulation study. *Phys. Rev. E: Stat. Phys., Plasmas, Fluids, Relat. Interdiscip. Top.* **1996**, *53*, 5063−5074.
(36) Brown, S.; Szamel, G. Structure and dynamics of ring polymers. *J. Chem. Phys.* **1998**, *108*, 4705−4708.
(37) Brown, S.; Szamel, G. Computer simulation study of the structure and dynamics of ring polymers. *J. Chem. Phys.* **1998**, *109*, 6184−6192.
(38) Halverson, J. D.; Lee, W. B.; Grest, G. S.; Grosberg, A. Y.; Kremer, K. Molecular dynamics simulation study of nonconcatenated ring polymers in a melt. I. Statics. *J. Chem. Phys.* **2011**, *134*, 204904.
(39) Tsalikis, D. G.; et al. Microscopic Structure, Conformation, and Dynamics of Ring and Linear Poly(ethylene oxide) Melts from

https://dx.doi.org/10.1021/acs.macromol.9b02706
Macromolecules 2020, 53, 3390−3408

Detailed Atomistic Molecular Dynamics Simulations: Dependence on Chain Length and Direct Comparison with Experimental Data. *Macromolecules* **2017**, *50*, 2565−2584.
(40) Richter, D.; Gooßen, S.; Wischnewski, A. Celebrating Soft Matter's 10th Anniversary: Topology matters: structure and dynamics of ring polymers. *Soft Matter* **2015**, *11*, 8535−8549.
(41) Hur, K.; et al. Chain Dynamics of Ring and Linear Polyethylene Melts from Molecular Dynamics Simulations. *Macromolecules* **2011**, *44*, 2311−2315.
(42) Lee, E.; Kim, S.; Jung, Y. Slowing Down of Ring Polymer Diffusion Caused by Inter-Ring Threading. *Macromol. Rapid Commun.* **2015**, *36*, 1115−1121.
(43) Ge, T.; Panyukov, S.; Rubinstein, M. Self-Similar Conformations and Dynamics in Entangled Melts and Solutions of Nonconcatenated Ring Polymers. *Macromolecules* **2016**, *49*, 708−722.
(44) Halverson, J. D.; Lee, W. B.; Grest, G. S.; Grosberg, A. Y.; Kremer, K. Molecular dynamics simulation study of nonconcatenated ring polymers in a melt. II. Dynamics. *J. Chem. Phys.* **2011**, *134*, 204905.
(45) Kapnistos, M.; et al. Unexpected power-law stress relaxation of entangled ring polymers. *Nat. Mater.* **2008**, *7*, 997−1002.
(46) Pasquino, R.; et al. Viscosity of Ring Polymer Melts. *ACS Macro Lett.* **2013**, *2*, 874−878.
(47) Doi, Y.; et al. Melt Rheology of Ring Polystyrenes with Ultrahigh Purity. *Macromolecules* **2015**, *48*, 3140−3147.
(48) Smrek, J.; Grosberg, A. Y. Understanding the dynamics of rings in the melt in terms of the annealed tree model. *J. Phys.: Condens. Matter* **2015**, *27*, 064117.
(49) Edwards, S. F. Statistical mechanics with topological constraints: I. *Proc. Phys. Soc., London* **1967**, *91*, 513−519.
(50) Edwards, S. F. Statistical mechanics with topological constraints: II. *J. Phys. A: Math. Gen.* **1968**, *1*, 303.
(51) Frank-Kamenetskii, M. D.; Lukashin, A. V.; Vologodskii, A. V. Statistical mechanics and topology of polymer chains. *Nature* **1975**, *258*, 398−402.
(52) Iwata, K.; Kimura, T. Topological distribution functions and the second virial coefficients of ring polymers. *J. Chem. Phys.* **1981**, *74*, 2039−2048.
(53) Tanaka, F. Osmotic pressure of ring-polymer solutions. *J. Chem. Phys.* **1987**, *87*, 4201−4206.
(54) Weidmann, J.-L.; et al. Poly[2]catenanes and Cyclic Oligo[2]-catenanes Containing Alternating Topological and Covalent Bonds: Synthesis and Characterization. *Chem. - Eur. J.* **1999**, *5*, 1841−1851.
(55) Bruns, C. J.; Stoddart, J. F. *The Nature of the Mechanical Bond: From Molecules to Machines*; John Wiley & Sons, Inc., 2016. DOI: 10.1002/9781119044123.
(56) Wasserman, E. The Preparation of Interlocking Rings: A Catenane. *J. Am. Chem. Soc.* **1960**, *82*, 4433−4434.
(57) Nierengarten, J. F.; Dietrich-Buchecker, C. O.; Sauvage, J. P. Synthesis of a Doubly Interlocked [2]-Catenane. *J. Am. Chem. Soc.* **1994**, *116*, 375−376.
(58) McArdle, C. P.; Vittal, J. J.; Puddephatt, R. J. Molecular Topology: Easy Self-Assembly of an Organometallic Doubly Braided [2]Catenane. *Angew. Chem.* **2000**, *112*, 3977−3980.
(59) Pentecost, C. D.; et al. A Molecular Solomon Link. *Angew. Chem., Int. Ed.* **2007**, *46*, 218−222.
(60) Mao, C.; Sun, W.; Seeman, N. C. Assembly of Borromean rings from DNA. *Nature* **1997**, *386*, 137−138.
(61) Chichak, K. S.; et al. Molecular Borromean rings. *Science* **2004**, *304*, 1308−1312.
(62) Arunachalam, M.; Gibson, H. W. Recent developments in polypseudorotaxanes and polyrotaxanes. *Prog. Polym. Sci.* **2014**, *39*, 1043−1073.
(63) Niu, Z.; Gibson, H. W. Polycatenanes. *Chem. Rev.* **2009**, *109*, 6024−6046.
(64) Noda, Y.; Hayashi, Y.; Ito, K. From topological gels to slide-ring materials. *J. Appl. Polym. Sci.* **2014**, *131*, 40509.
(65) Mena-Hernando, S.; Pérez, E. M. Mechanically interlocked materials. Rotaxanes and catenanes beyond the small molecule. *Chem. Soc. Rev.* **2019**, *48*, 5016−5032.
(66) Wu, Q.; et al. Poly[n]catenanes: Synthesis of molecular interlocked chains. *Science* **2017**, *358*, 1434−1439.
(67) Pakula, T.; Jeszka, K. Simulation of Single Complex Macromolecules. 1. *Macromolecules* **1999**, *32*, 6821−6830.
(68) Rauscher, P. M.; Rowan, S. J.; de Pablo, J. J. Topological Effects in Isolated Poly[n]catenanes: Molecular Dynamics Simulations and Rouse Mode Analysis. *ACS Macro Lett.* **2018**, *7*, 938−943.
(69) Brereton, M. G. The statistical mechanics of a concatenated polymer chain. *J. Phys. A. Math. Gen.* **2001**, *34*, 5131.
(70) Sikorski, A. Monte Carlo study of catenated ring polymers. *Polymer* **1994**, *35*, 3792−3794.
(71) Tsolou, G.; Stratikis, N.; Baig, C.; Stephanou, P. S.; Mavrantzas, V. G. Melt Structure and Dynamics of Unentangled Polyethylene Rings: Rouse Theory, Atomistic Molecular Dynamics Simulation, and Comparison with the Linear Analogues. *Macromolecules* **2010**, *43*, 10692−10713.
(72) Rouse, P. E. A Theory of the Linear Viscoelastic Properties of Dilute Solutions of Coiling Polymers. *J. Chem. Phys.* **1953**, *21*, 1272−1280.
(73) Wu, Z.-T.; Zhou, J.-J. Mechanical Properties of Interlocked-ring Polymers: A Molecular Dynamics Simulation Study. *Chin. J. Polym. Sci.* **2019**, *37*, 1298−1304.
(74) Reid, D. R.; Helffrich, J.; Webb, M. A.; Andreev, M.; Keene, B. P.; Rauscher, P. M.; Wyetzner, S.; de Pablo, J. J. *DASH*; MICCoM Codes, 2016. http://miccomcodes.org/index.html.
(75) Bohn, M.; Heermann, D. W. Topological interactions between ring polymers: Implications for chromatin loops. *J. Chem. Phys.* **2010**, *132*, 044904.
(76) Zimm, B. H.; Stockmayer, W. H. The dimensions of chain molecules containing branches and rings. *J. Chem. Phys.* **1949**, *17*, 1301−1314.
(77) Müller, M.; Wittmer, J. P.; Cates, M. E. Topological effects in ring polymers. II. Influence of persistence length. *Phys. Rev. E: Stat. Phys., Plasmas, Fluids, Relat. Interdiscip. Top.* **2000**, *61*, 4078−4089.
(78) Suzuki, J.; Takano, A.; Matsushita, Y. Dimensions of catenated ring polymers in dilute solution studied by Monte-Carlo simulation. *J. Chem. Phys.* **2018**, *149*, 204901.
(79) Bohn, M.; Heermann, D. W.; Lourenço, O.; Cordeiro, C. On the Influence of Topological Catenation and Bonding Constraints on Ring Polymers. *Macromolecules* **2010**, *43*, 2564−2573.
(80) Wittmer, J. P.; et al. Long range bond-bond correlations in dense polymer solutions. *Phys. Rev. Lett.* **2004**, *93*, 147801.
(81) Wittmer, J. P.; et al. Intramolecular long-range correlations in polymer melts: The segmental size distribution and its moments. *Phys. Rev. E* **2007**, *76*, 011803.
(82) Zhao, S. R.; Sun, C. P.; Zhang, W. X. Statistics of wormlike chains. I. Properties of a single chain. *J. Chem. Phys.* **1997**, *106*, 2520−2529.
(83) Hsu, H.-P.; Paul, W.; Binder, K. Polymer chain stiffness vs. excluded volume: A Monte Carlo study of the crossover towards the worm-like chain model. *Europhys. Lett.* **2010**, *92*, 28003.
(84) Hsu, H.-P.; Paul, W.; Rathgeber, S.; Binder, K. Characteristic Length Scales and Radial Monomer Density Profiles of Molecular Bottle-Brushes: Simulation and Experiment. *Macromolecules* **2010**, *43*, 1592−1601.
(85) Messmer, D.; et al. 3D Conformations of Thick Synthetic Polymer Chains Observed by Cryogenic Electron Microscopy. *ACS Nano* **2019**, *13*, 3466−3473.
(86) Grosberg, A. Y. Critical exponents for random knots. *Phys. Rev. Lett.* **2000**, *85*, 3858−3861.
(87) Halverson, J. D.; Smrek, J.; Kremer, K.; Grosberg, A. Y. From a melt of rings to chromosome territories: the role of topological constraints in genome folding. *Rep. Prog. Phys.* **2014**, *77*, 022601.
(88) de Gennes, P. G. *Scaling Concepts in Polymer Physics*; Cornell University Press, 1979.

https://dx.doi.org/10.1021/acs.macromol.9b02706
Macromolecules 2020, 53, 3390−3408

(89) Rubinstein, M.; Colby, R. H. *Polymer Physics*; Oxford University Press, 2003.
(90) Dell, Z. E.; Schweizer, K. S. Intermolecular structural correlations in model globular and unconcatenated ring polymer liquids. *Soft Matter* **2018**, *14*, 9132−9142.
(91) Porod, G. Die Röntgenkleinwinkelstreuung von dichtgepackten kolloiden Systemen. *Colloid Polym. Sci.* **1951**, *124*, 83−114.
(92) Ruland, W. Small-angle scattering of two-phase systems: determination and significance of systematic deviations from Porod's law. *J. Appl. Crystallogr.* **1971**, *4*, 70−73.
(93) Sinha, S. K.; Sirota, E. B.; Garoff, S.; Stanley, H. B. X-ray and neutron scattering from rough surfaces. *Phys. Rev. B: Condens. Matter Mater. Phys.* **1988**, *38*, 2297−2311.
(94) Banaszak, B. J.; de Pablo, J. J. A new double-rebridging technique for linear polyethylene. *J. Chem. Phys.* **2003**, *119*, 2456−2462.
(95) Auhl, R.; Everaers, R.; Grest, G. S.; Kremer, K.; Plimpton, S. J. Equilibration of long chain polymer melts in computer simulations. *J. Chem. Phys.* **2003**, *119*, 12718−12728.
(96) Sliozberg, Y. R.; Andzelm, J. W. Fast protocol for equilibration of entangled and branched polymer chains. *Chem. Phys. Lett.* **2012**, *523*, 139−143.
(97) Subramanian, G. A topology preserving method for generating equilibrated polymer melts in computer simulations. *J. Chem. Phys.* **2010**, *133*, 164902.
(98) Berendsen, H. J. C.; Postma, J. P. M.; van Gunsteren, W. F.; DiNola, A.; Haak, J. R. Molecular dynamics with coupling to an external bath. *J. Chem. Phys.* **1984**, *81*, 3684−3690.

https://dx.doi.org/10.1021/acs.macromol.9b02706
Macromolecules 2020, 53, 3390−3408